JGR Oceans

RESEARCH ARTICLE
10.1029/2023JC020699

Assessing Winter Phytoplankton Community Composition Dynamics and Their Response to Environmental Drivers in the Subarctic Northeast Pacific

Perumthuruthil Suseelan Vishnu[1,2], Justin Del Bel Belluz[3], M. Angelica Peña[4], Brian P. V. Hunt[5], Anna Vazhova[6], Midhun Shah Hussain[7], Hongyan Xi[8], Astrid Bracher[8,9], and Maycira Costa[1]

[1]SPECTRAL Remote Sensing Laboratory, Department of Geography, University of Victoria, Victoria, BC, Canada, [2]Department of Engineering Cybernetics, Norwegian University of Science and Technology, Trondheim, Norway, [3]Hakai Institute, Victoria, BC, Canada, [4]Fisheries and Oceans Canada, Institute of Ocean Sciences, Sidney, BC, Canada, [5]Institute for the Oceans and Fisheries and Department of Earth, Ocean, and Atmospheric Sciences, University of British Columbia, Vancouver, BC, Canada, [6]Pacific Branch of the Federal State Budget Scientific Institution of Fisheries and Oceanography, Vladivostok, Russia, [7]Department of Marine Biology, Microbiology, and Biochemistry, Cochin University of Science and Technology, Cochin, Kerala, India, [8]Phytooptics Group, Physical Oceanography of Polar Seas, Climate Sciences, Alfred Wegener Institute, Helmholtz Centre for Polar and Marine Research, Bremerhaven, Germany, [9]Department of Physics and Electrical Engineering, Institute of Environmental Physics, University of Bremen, Bremen, Germany

Abstract The subarctic northeast Pacific (SNEP) is a high-nutrient, low-chlorophyll region where primary productivity is limited by bioavailable iron during the spring through autumn, and by light limitation during winter. Here, we investigate the spatio-temporal distribution and drivers of SNEP surface phytoplankton biomass and community composition in the winters of 2019 and 2020 using in situ environmental data, chemotaxonomic analysis of phytoplankton pigment samples, and Sentinel-3A Ocean Land Color Instrument imagery. The utilized satellite-based algorithm showed promise replicating the expected trends of: (a) homogenous phytoplankton communities dominated by haptophytes, green algae, and pelagophytes in highly mixed light-limited oceanic waters and; (b) increased diatoms in coastal Haida Gwaii waters with reduced mixed-layer depth (MLD) and salinity. Unexpectedly, increases in cryptophytes were observed in the northern extents of the SNEP, which coincided with winter marine heatwave driven reductions in MLDs and also the presence of a mesoscale eddy. This finding highlights a deviation from expected homogeneous phytoplankton conditions, which may be systematically missed by spatially and temporally constrained in situ sampling. The further advancement and deployment of the satellite-based algorithm could significantly expand the understanding of winter phytoplankton dynamics in the SNEP, a critical period for Pacific salmon survival, improving the understanding of trophic linkages and match/mismatch dynamics, and contributing to improve the forecasting of salmon returns.

Plain Language Summary Phytoplankton are the foundation of the marine food web, significantly regulating biogeochemical processes and contributing to about half of the global primary productivity. Therefore, monitoring phytoplankton community composition is critical for understanding the ocean's role in climate change and fisheries. Satellite observations are more cost-effective than ship-based observations, with a much higher spatial and temporal resolution. Here, we combined field-collected samples of phytoplankton pigments and satellite imagery to estimate phytoplankton composition in the winter of 2019 and 2020 across the northeast Pacific. The satellite outputs aligned well with field data, giving confidence to this method. Generally low biomass and consistent phytoplankton communities, dominated by small flagellates called haptophytes, were observed across varying environmental conditions over these iron-limited open ocean regions. Diatoms were more prevalent near Haida Gwaii, where iron availability was likely higher and mixing was less pronounced, likely increasing light availability for the growth of these large species. Additionally, cryptophytes increased in the northern study area, possibly due to the influence of a marine heatwave and a mesoscale eddy. This study showcases the potential application of satellite imagery for investigating phytoplankton community composition over the subarctic northeast Pacific, which provides habitats for various commercially important pelagic fisheries, including Pacific salmon.

Key Points:

- Satellite ocean color and in situ data characterized winter surface phytoplankton community composition across the northeast Pacific
- Increased cryptophyte biomass was observed during marine heatwave conditions and the presence of an eddy
- The employed method expands the limited winter phytoplankton composition data from an undersampled region vital for Pacific salmon survival

Supporting Information:

Supporting Information may be found in the online version of this article.

Correspondence to:

P. S. Vishnu,
psvishnu2014@gmail.com

Citation:

Vishnu, P. S., Del Bel Belluz, J., Peña, M. A., Hunt, B. P. V., Vazhova, A., Hussain, M. S., et al. (2025). Assessing winter phytoplankton community composition dynamics and their response to environmental drivers in the subarctic northeast Pacific. *Journal of Geophysical Research: Oceans*, *130*, e2023JC020699. https://doi.org/10.1029/2023JC020699

Received 10 NOV 2023
Accepted 22 MAY 2025

Author Contributions:

Conceptualization: Perumthuruthil Suseelan Vishnu, Maycira Costa
Formal analysis: Perumthuruthil Suseelan Vishnu
Funding acquisition: Maycira Costa
Investigation: Perumthuruthil Suseelan Vishnu
Methodology: Perumthuruthil Suseelan Vishnu, Justin Del Bel Belluz, Midhun Shah Hussain, Hongyan Xi, Astrid Bracher
Software: Perumthuruthil Suseelan Vishnu
Supervision: Maycira Costa

Validation: Perumthuruthil Suseelan Vishnu
Visualization: Perumthuruthil Suseelan Vishnu, Justin Del Bel Belluz
Writing – original draft: Perumthuruthil Suseelan Vishnu
Writing – review & editing: Justin Del Bel Belluz, M. Angelica Peña, Brian P. V. Hunt, Anna Vazhova, Midhun Shah Hussain, Hongyan Xi, Astrid Bracher, Maycira Costa

1. Introduction

Phytoplankton, as the foundation of the marine food web play a central role in the functioning of the global ocean by driving the biological carbon pump through the export of carbon to deep waters, thereby sustaining nutrient cycling and facilitating elemental exchange with the atmosphere (e.g., Hood et al., 2006; Le Quéré et al., 2005). These biogeochemical functions (e.g., silicification, calcification, nitrogen fixation, and export flux) are strongly dependent on the composition and size structure of phytoplankton communities (Le Quéré et al., 2005). For example, microphytoplankton, such as diatoms, are the predominant silicifiers in the ocean and are responsible for transporting carbon, nitrogen, and silicate into the deep waters (Benoiston et al., 2017; Taucher et al., 2022; Tréguer et al., 2018). Furthermore, phytoplankton size structure often exhibits a direct link with fisheries; in the Benguela upwelling ecosystem, for example, small-sized flagellate communities supported the growth of sardines, whereas diatoms supported the growth of anchovies (Cury et al., 2008). As a result, shifts in phytoplankton community composition and size structure can have significant implications for oceanic elemental cycling and the transfer of energy to higher trophic communities, including commercially and culturally important fish populations (e.g., Beardall & Raven, 2004; Beardall & Stojkovic, 2006; Dutkiewicz et al., 2020; Falkowski & Oliver, 2007; Le Quéré et al., 2005; Legendre, 1990; Petrou et al., 2016; Stock et al., 2014; Vanni & Findlay, 1990). Therefore, monitoring phytoplankton community composition in global and regional ocean waters is paramount to inform how phytoplankton respond to changing climate and their potential implication on fisheries production and ocean biogeochemistry.

Understanding phytoplankton community dynamics is especially important for the subarctic northeast Pacific (SNEP), which is considered a high-nutrient, low-chlorophyll (HNLC) region where phytoplankton growth is limited by bioavailable iron (BFe) (Harrison et al., 2004; Peña & Varela, 2007). In this region, total Chlorophyll-a (hereafter TChla, a proxy for phytoplankton biomass; McClain, 2009) is generally low (<0.5 mg m^{-3}) and invariant, despite marked seasonality in nutrient concentrations and primary productivity (e.g., Evans & Parslow, 1985; Peña et al., 2019; Peña & Varela, 2007; Vinogradov et al., 1997; Westberry et al., 2016); however, sporadic blooms can occur due to the introduction of BFe into the mixed layer (Hamme et al., 2010). Beyond the availability of BFe, phytoplankton growth and production in the subarctic gyre largely depend on irradiance, vertical mixing, and grazing pressure (Aguilar-Islas et al., 2016; Dagg et al., 2009; Harrison et al., 2004; Henson, 2007). In winter, strong vertical mixing brings inorganic nutrients (nitrate and silicate) and BFe into the mixed layer, but also transports phytoplankton below the euphotic depth, limiting light exposure required for growth (Harrison et al., 2004; Peña & Varela, 2007).

Primary productivity in the SNEP is estimated to be 170 g C m^2/y (Welschmeyer et al., 1993). The community composition that makes up this productivity has been investigated using various methods, including microscopy, high-performance liquid chromatography (HPLC) phytoplankton pigment concentrations and corresponding chemical taxonomy (CHEMTAX), and physical-biological models (e.g., Booth et al., 1993; Fujiki et al., 2009; Harrison et al., 2004; Peña et al., 2019; Peterson et al., 2011; Peterson & Harrison, 2012; Zhang et al., 2021). Among the numerous in situ techniques used, conventional light microscopy excels at identifying phytoplankton to either genus or species level and is effective for enumeration and identification of microphytoplankton (>10 μm) but generally misses smaller-sized species that are regionally important (Brito et al., 2015; Del Bel Belluz et al., 2024; Goela et al., 2014). As a result, studies have largely relied on HPLC pigment data and corresponding CHEMTAX analysis to characterize phytoplankton community composition at a broad functional group level (e.g., Fujiki et al., 2009; Peña et al., 2019; Peterson & Harrison, 2012; Taves et al., 2022). This method can resolve groups containing small nano- and pico-sized species (<10 μm) including those shown to dominate in the SNEP (e.g., Haptophytes) (Del Bel Belluz et al., 2021; Peña et al., 2019; Vaillancourt et al., 2018). Despite the utility of these in situ methods, they are generally time-consuming, labor-intensive, expensive, and, most importantly, limited in space and time. Alternatively, combining Earth Observation satellites and in situ techniques can address the limitations of monitoring the spatial and temporal distribution of phytoplankton community composition in the SNEP (Konik et al., 2024; Vishnu et al., 2022).

Satellite-based methods have been developed for determining phytoplankton group and size classes in the ocean using abundance-based (e.g., Brewin et al., 2010, 2015; Hirata et al., 2011; Uitz et al., 2006), radiance/reflectance-based (e.g., Alvain et al., 2005; Bracher et al., 2009; Werdell et al., 2014; Xi et al., 2020), and backscattering-based methods (e.g., Kostadinov et al., 2009, 2010). An alternative satellite-based approach employs Empirical Orthogonal Function (EOF) analysis on remote sensing reflectance Rrs(λ) and derived

accessory pigment concentrations (e.g., Bracher et al., 2015; Craig et al., 2012; Lubac & Loisel, 2007; Soja-Woźniak et al., 2017), Chlorophyll-a (hereafter Chl a) concentrations of multiple phytoplankton groups (e.g., Vishnu et al., 2022; Xi et al., 2020), or phytoplankton community abundances (e.g., Lange et al., 2020). Previous studies have used EOF algorithms to retrieve phytoplankton groups and accessory pigments from multispectral reflectance data using a compilation of global data sets (e.g., Xi et al., 2020, 2021); however, these global algorithms often have poor regional performance due to insufficient representation of local data. Regional studies require algorithm fine-tuning, validation, and careful analysis to reduce error and produce results suitable for advancing the understanding of phytoplankton dynamics (Konik et al., 2024). Considerable research has been done on SNEP phytoplankton dynamics; however, much of the phytoplankton compositional work has been derived from spatio-temporally constrained in situ samples (e.g., Fujiki et al., 2009; Peña et al., 2019). The development of satellite-based algorithms for retrieving phytoplankton communities in the North Pacific can help address this shortcoming (Konik et al., 2024). In particular, further efforts are needed during the data-poor winter period, when fundamental understanding of the system remains limited. These data are important to understanding winter food web dynamics for Pacific salmon, with winter hypothesized to be a critical period for their survival (Beamish & Mahnken, 2001; Trudel et al., 2011).

In this study, we aimed to further the understanding of winter phytoplankton community composition (PCC) dynamics in the SNEP by integrating multiple data sets collected during the International Year of Salmon cruise, which took place in the winter of 2019 and 2020 in the Gulf of Alaska. Specifically, we combined PCC data from Sentinel-3 OLCI, pigment-based PCC (CHEMTAX), and physicochemical data to: (a) assess the applicability of the satellite-based PCC retrievals; (b) use the combined data set to characterize winter phytoplankton communities across large spatial-scales and; (c) investigate their environmental drivers. To our knowledge, no such integrated phytoplankton community composition data sets exist for this region during the winter season, which is hypothesized to be a crucial period for the foraging success and survival of Pacific salmon overwintering in the North Pacific. Based on the available research and the low light and highly mixed conditions, we hypothesized low biomass and homogenous surface communities throughout the region during this season; however, our unique high spatio-temporal data set would have allowed us to capture deviations from this homogeneity with potential ecological importance. This study provides a baseline for future research investigating regional links between PCC and the food web, with implications for species such as Pacific salmon.

2. Materials and Methods

2.1. Study Area

The SNEP is generally considered north of 45°N and includes the open ocean basin, continental shelf, and coastal margins of Alaska and British Columbia (BC) (Figure 1). Within the SNEP, the ocean circulation and phytoplankton communities in the open ocean region of the Gulf of Alaska (GoA) are distinct from the coastal and continental shelf margin of Alaska and BC (e.g., Booth et al., 1993; Fujiki et al., 2009; Peña & Varela, 2007; Peña et al., 2019; Weingartner et al., 2009). The Alaska Gyre dominates the circulation in the open ocean, a component of the broad subarctic gyre in the North Pacific Ocean (Weingartner, 2006; Weingartner et al., 2002). This cyclonic gyre consists of the eastward-flowing North Pacific Current, the northwest-flowing Alaska Current, and the westward-flowing Alaska Stream (Stabeno et al., 2004; Weingartner et al., 2009). The circulation of the gyre is driven by counter-clockwise winds, which initiate surface Ekman transport, leading to upwelling in the central GoA and downwelling toward the continental shelf margin (Weingartner, 2006). The central GoA shows high phytoplankton diversity largely comprising small (<10 μm) haptophytes, green algae, and pelagophytes (e.g., Booth et al., 1993; Fujiki et al., 2009; Peña et al., 2019) that can survive in the iron-poor open ocean waters (Peña & Varela, 2007). Productivity in this area is variable and linked to mesoscale eddies (Crawford, 2005), particularly Haida and Sitka eddies transporting heat, iron-rich coastal waters, and marine organisms to the open ocean waters of the GoA (Ueno et al., 2023). Moreover, climate forcings, such as El-Nino Southern Oscillations (ENSO) (Schwing et al., 2002), Pacific Decadal Oscillation (PDO), and the North Pacific Gyre Oscillation (NPGO) play an important role in regulating year-to-year variability in nutrients and primary production (Chavez et al., 2003; Di Lorenzo et al., 2008; Matua & Hare, 2002). Understanding this variability has important implications for fisheries, as the SNEP supports overwintering Pacific salmon populations originating from Canada, the United States, Russia, Japan, and Korea (Beamish, 2017).

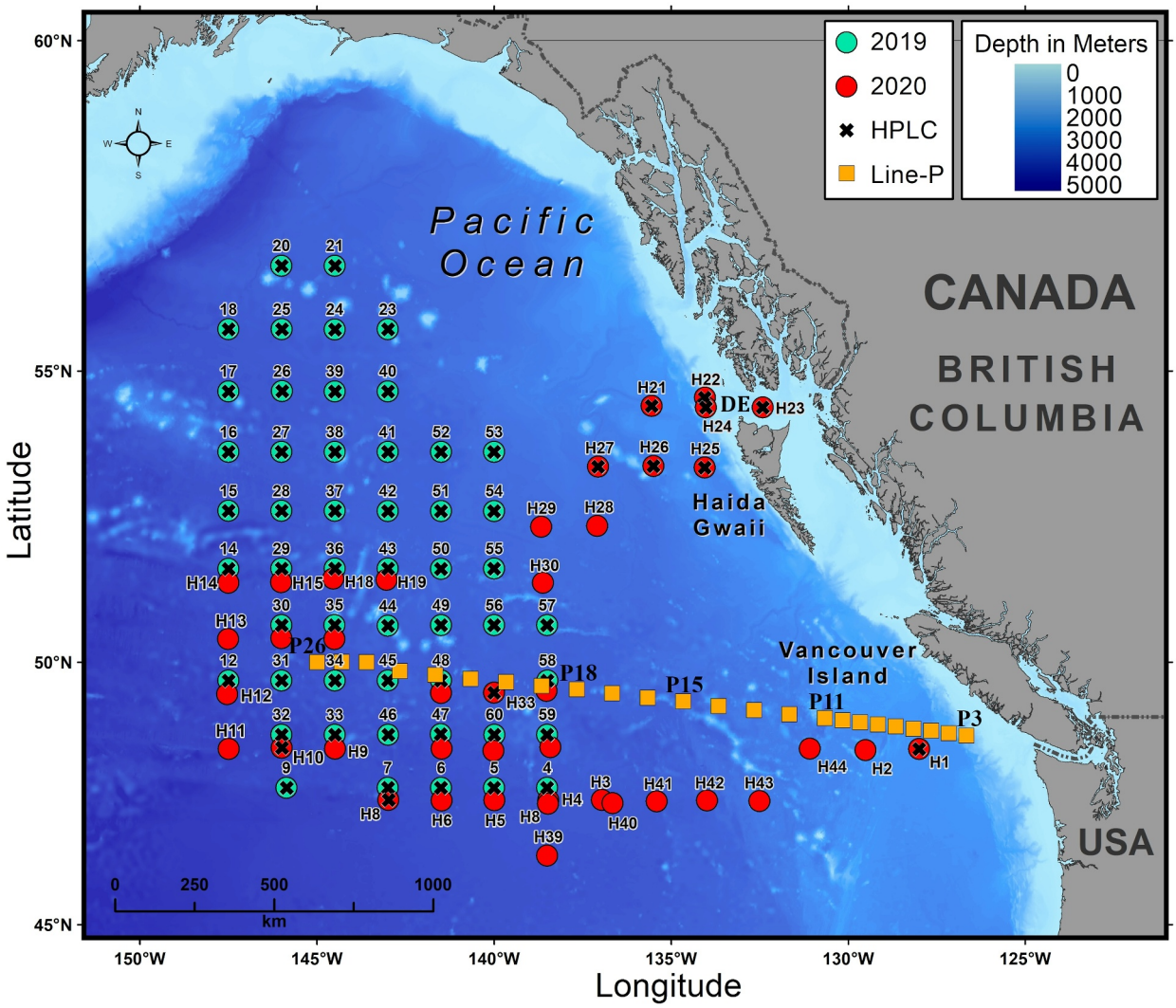

Figure 1. Map showing the sampling locations in the subarctic northeast Pacific. Green and red circles represent field stations for all physical and chemical variables sampled in 2019 and 2020, respectively. The symbol "X" indicates high performance liquid chromatography (HPLC)-pigments field stations for 2019 and 2020. Yellow squares denote the Line-P monitoring stations sampled by Fisheries and Oceans Canada (DFO), Canada. "DE" refers to Dixon Entrance. Bathymetry is shown in meters.

In contrast to the more oceanic waters, the continental shelf of the GoA is dominated by the Alaska Coastal Current (ACC), which is driven by wind and freshwater runoff and is responsible for the advection of dissolved nutrients, phytoplankton, and other organisms across the shelf (Royer, 1983; Stabeno et al., 1995, 2016). This coastal-influenced shelf region is highly productive, with annual primary productivity exceeding 300 g C/m^2/y (e.g., Sambrotto & Lorenzen, 1987; Siddon et al., 2019) supporting numerous commercially important fish species including Pacific Cod (*Gadus macrocephalus*), Walleye Pollock (*Gadus chalcogrammus*), Pacific Ocean Perch (*Sebastes alutus*), Pacific herring (*Clupea pallasii*), Arrowtooth Flounder (*Atheresthes stomias*) (Budge et al., 2022; Johnson et al., 2012; McGowan et al., 2019; Siddon et al., 2019), and various marine mammals (Womble et al., 2009; Womble & Sigler, 2006), and sea birds (Dragoo et al., 2017). Large phytoplankton, such as diatoms, dominate the coastal and continental shelf domains of the GoA and BC, with seasonal spring blooms reaching TChla concentrations >3 mg m^{-3} (e.g., Giannini et al., 2021; Jackson et al., 2015; MacNeil et al., 2024; Marchese et al., 2022; Peña & Nemcek, 2020; Peña et al., 2019; Peterson & Harrison, 2012; Pramlall et al., 2023; Strom et al., 2016; Suchy et al., 2019; Vishnu et al., 2022; Waite & Mueter, 2013). Additionally, this region is highly dynamic, showing strong seasonal, spatial, and interannual variability in TChla (e.g., Brickley & Thomas, 2004; Waite & Mueter, 2013), with spring bloom timing varying spatially and interannually (Marchese et al., 2022; Pramlall et al., 2024; Suchy et al., 2019).

2.2. Field Data

Data were acquired as part of the International Year of Salmon Expedition to the GoA onboard the Research Vessel *Professor Kaganovsky* (18 February to 21 March 2019) and the Research Vessel *Pacific Legacy* (5 March to 5 April 2020). At each station, conductivity-temperature-depth (CTD) profiles were performed, and surface (~1–5 m depth) water samples for phytoplankton pigments, dissolved oxygen, and macronutrient concentrations were collected using a CTD/rosette system equipped with Niskin bottles. The following section describes the methods for processing CTD, dissolved oxygen, macronutrients, phytoplankton pigments, and satellite data. Then, the training and implementation of the EOF-based algorithms used to retrieve phytoplankton community composition from weekly composite imagery are described, along with the statistical methods performed to investigate their physical and chemical drivers.

2.2.1. Environmental Variables

Continuous CTD profiles for both expeditions were performed with a Seabird SBE 911plus system with dual temperature and conductivity (salinity) and oxygen sensors. These sensors were calibrated before the commencement of each expedition to ensure high-quality data. Prior to analysis, the CTD data were aggregated into 1-m-depth bins. Based on the temperature and salinity data set, we used the Gibbs Sea Water Function from the R *gsw* package (Kelley & Richards, 2021) to calculate potential density, which was further used to derive the mixed layer depth (MLD) by calculating the depth at which the potential density was 0.1 kg m^{-3} greater than the surface value (Plant et al., 2016).

Dissolved oxygen (DO) measurements were conducted using different methodologies for the two expeditions. In 2019, DO was measured using the iodometric method, a modified version of Winkler's titration-based technique (Grasshoff et al., 1999), performed onboard. However, during the 2020 campaign, DO data were obtained directly from the calibrated CTD oxygen sensor.

Samples for the determination of nitrate (NO_2), nitrite (NO_3), phosphate (PO_4), and silicate (SiO_4) were collected at each station and transferred into 500 ml polyethylene bottles until analysis. During the 2019 campaign, analyses were conducted onboard using a Shimadzu UV-1800 spectrophotometer (with an error in transmission coefficient of ≤0.1%) without preliminary filtration, as the samples were free of suspended or colloidal substances. Nitrite (NO_2) and nitrate (NO_3) were quantified according to the method of Wood et al. (1967), where NO_2 is converted to NO_3 using a cadmium column. Phosphate (PO_4) levels were measured via the Murphy & Riley method at 885 nm, whereas silicate (SiO_4) was analyzed using the Dienert-Vandenbulcke method at 380 nm (Grasshoff et al., 1999). Measurement uncertainties were ±2.5% for NO_2, ±3.0% for NO_3, ±2.0% for PO_4, and ±2.8% for SiO_4, based on repeated analyses and certified reference materials (CRMs). For the 2020 campaign, inorganic nutrient samples were stored at −20°C until analysis was performed onshore in the laboratory using a Lachat QuikChem 8500 Series 2 Flow Injection Analysis (FIA) System, employing methods similar to those used in 2019. The uncertainties for FIA measurements were ±1.5% for NO_2, ±2.0% for NO_3, ±1.2% for PO_4, and ±1.8% for SiO_4. Quality control protocols included regular analysis of blanks and CRMs, with detection limits of 0.02 μM for NO_2, 0.05 μM for NO_3, 0.01 μM for PO_4, and 0.1 μM for SiO_4. All measurements underwent blank correction and were validated through internal consistency checks.

2.2.2. Phytoplankton Pigments Concentration

Samples for determining phytoplankton pigments were collected during both expeditions ($n = 51$ and $n = 11$ for 2019 and 2020, respectively). After collection, sample water was transferred to opaque 10 L plastic bottles and directly filtered under dim light to avoid pigment degradation (Mueller et al., 2003). Two liters of sample water was vacuum filtered (≤5 mmHg) through 25 mm Whatman glass microfibre filters (GF/F) with 0.7 μm pore size, and following filtration, the filters were folded inwards, placed in plastic vials, and flash frozen in liquid nitrogen. The samples were stored at −80°C until laboratory analysis by HPLC was conducted at the University of South Carolina Baruch Institute of Marine and Coastal Sciences following Pinckney (2010) (https://phytoninja.com/lab-protocols/). Twenty-two pigments were identified, including TChla, chlorophyll c_3 ($chlc_3$), chlorophyll c_1c_2 ($chlc_{12}$), peridinin (peri), 19′butanoyloxyfucoxanthin (BF), fucoxanthin (fuco), 19′hexanoyloxyfucoxanthin (HF), neoxanthin (neo), prasinoxanthin (pras), violaxanthin (viola), diadinoxanthin (diad), antheraxanthin (anther), alloxanthin (allo), diatoxanthin (diat), lutein (lut), zeaxanthin (zea), gyroxanthin-diester (gyro), chlorophyll-b (chlb), chlorophyll-a allomer (chla allomer), chlorophyll-a prime (chla′), α-carotene, and β-carotene.

The HPLC TChla and accessory pigment concentrations were further used as inputs for CHEMTAX analysis. CHEMTAX optimizes input accessory pigment:TChla ratios to those of the field data through an iterative process to derive estimates of the Chl a concentration of multiple phytoplankton groups (Mackey et al., 1996). This approach has been used successfully in the SNEP to investigate the distribution of dominant phytoplankton groups (Fujiki et al., 2009; Peña et al., 2019; Peterson et al., 2011; Peterson & Harrison, 2012). Before the CHEMTAX analysis, phytoplankton pigment data were clustered based on the ratios of pigment:TChla to derive groupings of stations with similar pigment ratios (method described in Section 2.5). The input matrix used for clustering is shown in Figure S1 in Supporting Information S1, where rows represent stations and columns represent pigment:TChla ratios. These similar stations were then analyzed together in CHEMTAX to account for potential differences in pigment ratios due to light and environmental variability across the data set that can skew outputs (Swan et al., 2016). The analysis resulted in three clusters: cluster-1 comprised 51 stations within the open ocean waters that were entirely from 2019 and had relatively high ratios of BF and HF to TChla; cluster-2 showed only 4 stations from 2020 that were from the southern open ocean portion of the study region and, when compared to cluster-1, had higher pigment:TChla ratios for most pigments, but still showed the highest ratios with HF and BF; cluster-3 encompassed 7 sites from the 2020 campaign representing continental shelf influenced stations that had notably lower HF and BF to TChla ratios (Figure S2 in Supporting Information S1). Because of the low number of samples in cluster-2, we were forced to combine it with cluster-1 for the CHEMTAX analysis, but kept cluster-3 separate due to the distinct differences in pigment:TChla ratios (Figure S3 in Supporting Information S1). The following phytoplankton groups were included in the CHEMTAX analysis: cyanobacteria (Cyano), haptophytes (Hapto), pelagophytes (Pelago), prasinophytes (Prasino), chlorophytes (Chlor), cryptophytes (Crypto), dinoflagellates (Dino), and diatoms (Diatoms). The pigments utilized in the analysis were chlc3, chlc$_1$c$_2$, peri, BF, fuco, HF, pras, viola, allox, zea, lut, and chlb. Input groups and pigment ratios were the same as those used by Peña et al. (2019) and were taken from Higgins et al. (2011) with the same initial ratios applied to the CHEMTAX analysis for each cluster. The CHEMTAX analysis method was also comparable to Peña et al. (2019) following Wright et al. (2009), where the input ratios for each cluster were first randomized, creating slightly different starting points for 60 separate runs. For each cluster, the output ratios and group-level estimates from the runs with the 6 (of 60) lowest RMSE values were averaged and used for analysis. The averaged output ratios for each cluster are provided in the Supporting Information S1 (Tables S1 and S2 in Supporting Information S1).

2.3. Sentinel-3A OLCI Data

The Ocean Land Color Instrument (OLCI) onboard the Sentinel-3A satellite is a sensor with high spatial (300 m) and temporal resolution (daily), capable of acquiring water reflectance in 10 bands (400, 412, 443, 490, 510, 560, 620, 665, 674, and 681 nm) within the visible spectrum, along with an improved signal-to-noise ratio and the off-nadir pointing of the sensor swath to eliminate sun glint (Donlon et al., 2012). Level-1 full-resolution OLCI data from 18 February to 21 March 2019, and 5 March to 5 April 2020, were downloaded from the Sentinel-3 Marine CODA (Copernicus Online Data Access) web service and processed using POLYMER version 4.10 (Steinmetz et al., 2011). POLYMER processed daily Rrs(λ) images were weekly binned using SNAP (version 6.0) in batch mode using GPT (Graphics Processing Tool), resulting in a total of eight weekly composites (including 2019 and 2020 periods). Although binning, the following quality flags were applied: "Cloud," "Invalid," "Negative Backscattering" (BB), "Out-of-bounds," "Exception," "High Air Mass," and "Thick Aerosol" (Steinmetz et al., 2016) following the recommendation of Giannini et al. (2021) and Vishnu et al. (2022). Finally, the median Rrs(λ) calculated from each band was used for the analysis. Weekly binned composites were required as the spatial coverage was much increased when compared to the daily data: using weekly resolved data is generally accepted since it matches the temporal scale of phytoplankton phenology in the open ocean (Lange et al., 2020; Scott & Werdell, 2019). Specifically in the Alaska Gyre, no abrupt temporal and spatial changes in the phytoplankton biomass are typically observed, with minimum seasonal or inter-annual variability (Evans & Parslow, 1985; Peña & Varela, 2007; Vinogradov et al., 1997; Vishnu et al., 2022; Westberry et al., 2016). Therefore, our study used the weekly binned OLCI imagery for further analysis.

2.4. EOF-Based Algorithm

We adapted the EOF-based algorithm developed by Bracher et al. (2015) and globally applied by Xi et al. (2020) to retrieve the Chl a concentration of phytoplankton groups for the SNEP waters. The following steps were adopted to retrieve phytoplankton groups based on the EOF algorithm:

2.4.1. Input Data

CHEMTAX-derived Phytoplankton Community Composition: Before running the EOF algorithm CHEMTAX-derived data were grouped in two ways to improve satellite retrievals. First, the two green algae groups, chlorophytes, and prasinophytes, were combined and summed as it is unlikely that they could be separated via satellite due to similar pigment profiles. Second, the HPLC pigment ratios input into the CHEMTAX analysis were clustered by ratio (rather than station as was performed in Section 2.2.2, that is, pigment:TChla ratios input as rows and station as columns) to derive pigment groupings and thereby, CHEMTAX-derived outputs that showed similar trends (i.e., pigment collinearity). Under strong pigment collinearity, certain groups may not have been separable via satellite retrievals and this clustering approach indicates which groups could be combined to reduce error (Catlett & Siegel, 2018; Kramer & Siegel, 2019; Kramer et al., 2020). Methods for this clustering are described in Section 2.5. Clustering resulted in three broad groupings with pigments characteristic of: (a) Hapto/Pelago/Cyano; (b) Diatoms/Dino/GA; and (c) Crypto (Figure 2). For example, pigment:TChla ratios for HF, BF, chlc3, and zea clustered together, suggesting that haptophytes (chlc3, HF), pelagophytes (chlc3, BF), and cyanobacteria (zeaxanthin) covaried in the environment and may have been difficult to derive independently via satellite. Based on these pigment-based clustering results, we combined and summed the corresponding CHEMTAX-derived phytoplankton groups into broader groupings to improve accuracy, signal-to-noise ratio, and limit misclassifications of OLCI-derived phytoplankton groups. Next, the regression model was developed to estimate the Chl a concentration of each phytoplankton group (Hapto/Pelago/Cyano, Diatoms/Dino/GA, and Crypto), including TChla following Xi et al. (2020).

Rrs(λ): OLCI Rrs(λ) at the 10 OLCI bands were extracted from weekly composite imagery using 5 × 5 pixel windows centered on the location of the in situ sampling. The use of weekly composites is supported by Vishnu & Costa. (2023) who found no significant difference in TChla estimates between daily Sentinel-3 OLCI data (0.39 ± 0.08 mg m^{-3}) and weekly composites (0.38 ± 0.08 mg m^{-3}). More recently, Konik et al. (2024) employed weekly composited Rrs(λ) in the same EOF-based algorithm to retrieve phytoplankton functional groups across the North Pacific, successfully identifying distinct bioregions. In addition, weekly composites minimized the impact of cloud cover and data gaps, which are prominent in winter imagery, ensuring robust Rrs(λ) retrievals. For each 5 × 5 pixel window, the following quality control criteria were adopted: valid pixels were ≥17/25, the CV at 560 nm was ≤20%, and the median value from each band was used to avoid outliers (Mograne et al., 2019; Werdell & Bailey, 2005). Additionally, Rrs(λ) data outside the range of $\mu - 1.5\sigma$, $\mu + 1.5\sigma$, where μ is the mean and σ is the standard deviation, were excluded (Xi et al., 2020).

Furthermore, the final broad combined in situ CHEMTAX groupings (e.g., Diatoms/Dino/GA from step i) below ≤0.005 mg m^{-3} were removed from the analysis (Xi et al., 2020).

2.4.2. Algorithm Evaluation

Rrs(λ) spectra were used to compute the covariance matrix (C), and a singular value decomposition (SVD) was applied to derive three matrices: U (EOF scores), D (a diagonal matrix with singular values), and V (identified spectral patterns). Following this, a generalized linear model (GLM) was constructed between the $\log_{10}$-transformed CHEMTAX-derived phytoplankton group Chl a concentrations and the corresponding coefficients obtained from the product of U and D (Xi et al., 2020). Importantly, only significant patterns with singular values exceeding 0.001% of the highest value were included in the regression model (Xi et al., 2020). In turn, a stepwise optimization routine was implemented to identify the most significant predictors for the GLM by minimization of the Akaike information criteria (AIC) and the model performance was assessed using the coefficient of determination (R^2), mean absolute error (MAE; mg m^{-3}), median percentage difference (MDPD; %), and BIAS (%), with the corresponding equation detailed in Xi et al. (2020) and Vishnu et al. (2022). Subsequently, to ensure the robustness of the fitted regression model, a cross-validation approach was implemented by randomly splitting the data into 80% for training and 20% for testing, repeated for 500 permutations. Each iteration recorded R^2cv, MAEcv, and MDPDcv (Table 2). Finally, the regression model was applied to each weekly composite to generate spatial maps of phytoplankton groups. The full-fit and cross-validation statistical performance of the regression model is summarized in Table 2.

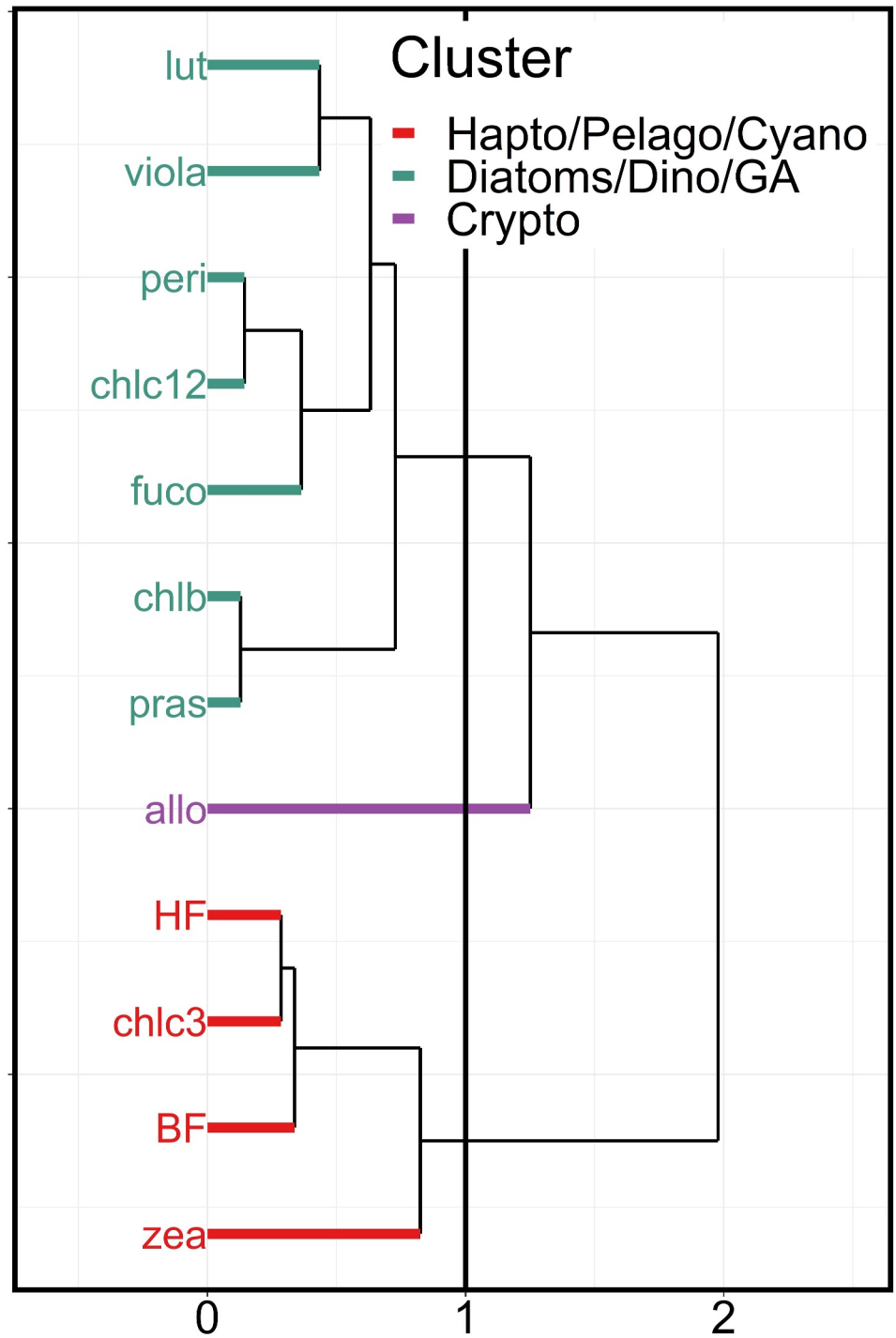

Figure 2. Hierarchical clustering of pigment:total Chlorophyll-a (TChla) ratios using the Pearson correlation distance and Ward's linkage method following Catlett and Siegel (2018), Kramer and Siegel (2019), and Kramer et al. (2020). The cophenetic correlation coefficient for the clustering was 0.74, indicating a good representation of the data (Kramer & Siegel, 2019). A linkage distance of 1 was used following Kramer and Siegel (2019) and Kramer et al. (2020) to define clusters. Different colors are used to show the three clusters, which are made up of pigments representing different phytoplankton groups.

2.4.3. Independent Validation

Semi-quantitative independent validation of the OLCI-derived TChla and PCC was assessed through comparison with in situ surface CHEMTAX-derived PCC data from the DFO Line-P monitoring program (Peña & Nemcek, 2021). The Line-P CHEMTAX analysis was performed using the same pigments and pigment ratios as here; however, the Line-P HPLC samples were analyzed using a different protocol, which may have introduced differences in outputs (Zapata vs. USC, see Nemcek & Peña, 2014). Furthermore, a direct 1:1 quantitative validation was not feasible due to the temporal mismatch between the data sets. For instance, in 2019, the OLCI phytoplankton group retrievals were obtained between February 18 and March 21, whereas the corresponding Line-P data were collected between February 6 and 12. Similarly, in 2020, the OLCI retrievals were derived between March 5 and April 5, whereas the Line-P data was collected from February 10 to 16. Considering these temporal mismatches, we only performed spatial matches with Line-P stations within the HNLC, outside of variable coastal influenced waters, where PCC is largely invariant over time (Line-P stations P3 to P26; see Figure 1) (Peña et al., 2019). The matchup extraction criteria and the statistical metrics used for the validation were the same as those used in the algorithm training (see input data in Section 2.4). Finally, the reliability of the satellite retrievals over a broader spatial and temporal domain was assessed through comparison to published results from previous studies in the SNEP. For this analysis, the composite with the highest spatial coverage was selected from 2019 to 2020. Spatio-temporal trends were extracted from a 5×5 pixel window within the weekly composite imagery across a latitudinal and longitudinal domain, and the corresponding standard deviation was presented.

2.5. Statistical Analyses

All statistical analyses were performed using R version 1.0.153 software (R Core Team, 2021; https://www.r-project.org/), and figures were created using ggplot2 (Wickham, 2016). Spatial maps for surface water properties and nutrients were created by interpolating discrete CTD stations using the bilinear interpolation method with the "Raster" package and the "disaggregate" functions. Additionally, contours were created by applying the "contour" function from the "Raster" package to the interpolated raster data. Finally, significant differences between the physical and chemical variables between 2019 and 2020 were determined using the nonparametric Wilcoxon Rank-Sum test using the "wilcox.test" function.

Pigment ratios were clustered in two different ways (see Sections 2.2.2 and 2.4), but both were performed using hierarchical clustering via the "stats" package and "dist" and "hclust" functions. First, the clustering to derive the CHEMTAX analysis groupings (Section 2.2.2) was done by station (i.e., station as rows and pigment ratios as columns) using Euclidean distances and Ward's linkage method (Ward.D2) following Swan et al. (2016). Selection of clusters was performed via visual inspection of the dendrogram and the Silhouette method visualized using the "fviz_nbclust" function from the "factoextra" package. Second, the hierarchical clustering performed to assess pigment colinearity and derive broad satellite groupings (Section 2.4) was done by pigment ratio (i.e., pigment ratios as rows and stations as columns) using the correlation distance (1-R, where R is the Pearson correlation between the input pigment ratios) and Ward's linkage method (Ward.D2) (Catlett & Siegel, 2018; Kramer et al., 2020; Kramer & Siegel, 2019). In this hierarchical clustering, a cutoff linkage of 1 was used to derive clusters representing similar and covariant phytoplankton communities (Kramer et al., 2020). For both clustering approaches, the quality of the clustering was assessed using the cophenetic correlation coefficient derived using the "stats" package and the "cophenetic" and "cor" functions. Cophenetic correlations range from 0 to 1, with values close to 1 suggesting that the dendrogram accurately represented the distances between the input parameters (Legendre & Legendre, 1998).

Following the cluster analysis, redundancy analysis (RDA) was performed to investigate the role of environmental drivers on the CHEMTAX-derived and OLCI-derived phytoplankton groups, following methods by Vaillancourt et al. (2018) and Del Bel Belluz et al. (2021). Redundancy analysis was performed independently on the CHEMTAX data set ($n = 62$) and the OLCI outputs ($n = 62$). The response variables of the first analysis were the Chl a contributions of the eight CHEMTAX phytoplankton groups (Cyano, Hapto, Pelago, Prasino, Chlor, Crypto, Dino, and Diatoms). The second RDA analysis used the three significant OLCI phytoplankton groups (Hapto/Pelago/Cyano, Diatoms/Dino/GA, and Crypto). Explanatory variables for both analyses were the same: sea surface temperature (SST), sea surface salinity (SSS), potential density (sigma-t), mixed layer depth (MLD), surface dissolved oxygen (DO), dissolved inorganic nitrogen (DIN), dissolved inorganic phosphate (DIP), and dissolved silicate (DSi). Prior to each RDA analysis, the response variables were transformed using the Hellinger

transformation ("Vegan" package and "decostand" function), which makes taxonomic data more suitable for the linear RDA method and gives groups with low or zero contributions reduced weights (Legendre & Gallagher, 2001; Ramette, 2007). Furthermore, collinearity of explanatory variables, which can reduce the quality of RDA analysis, was checked using variance inflation factors (VIFs) (Vaillancourt et al., 2018) via the "vif.cca" function from the "vegan" package. Explanatory variables with the highest VIFs were removed until all remaining variables had VIF scores <10 (Mojica et al., 2015; Vaillancourt et al., 2018). Once the transformations and removals were complete, the RDAs were run using the "rda" function (vegan package) on the response and explanatory data sets to test for global significance (Ramette, 2007). After it was determined that the data were appropriate and the global models were significant (CHEMTAX: $p < 0.001$; OLCI: $p < 0.05$), forward selection of the explanatory variables was performed using the "OrdiR2step" function (vegan package) and Monte Carlo permutation (49,999) to determine and remove variables that did not significantly ($p > 0.05$) contribute to the variance (Blanchet et al., 2008; Ramette, 2007; Vaillancourt et al., 2018). Analysis was then run on only the significant variables to derive the final results.

Finally, the Kolmogorov-Smirnov test ("nortest" package) was used to evaluate the applicability of our regression between in situ and OLCI-derived phytoplankton group Chl a concentration (see Section 2.4).

3. Results

3.1. Physicochemical Properties

In general, most of the physicochemical properties in both years showed latitudinal (north to south) and longitudinal (east to west) gradients (Figures 3 and 4); however, distinct temporal differences were observed between years, with comparisons showing significant differences for all variables ($p < 0.05$, Wilcoxon Rank-Sum test).

In 2019 and 2020, SST varied latitudinally, with the 7°C isotherm delineating the boundary between the subarctic water mass to the northwest and the subtropical water mass to the southeast (Table 1; Figures 3a and 3b). Likewise, in both years, SSS mirrored the temperature distribution, with the 32.4 PSU isohaline marking the water mass boundary (Figure 3c; Table 1); however, in 2020, sampling extended eastward with lower salinities observed in coastal Vancouver Island waters and, most prominently, in Haida Gwaii shelf waters. For sigma-t, the 25.4 kg m^{-3} isoline followed the water mass boundary in both years, but in 2019, a localized low density feature was evident south of 55° N (Figure 3e), whereas in 2020, lower sigma-t values were observed toward the Haida Gwaii shelf waters and Vancouver Island. Unlike the other variables, MLD showed large differences between years. In 2019, MLDs were much shallower, ranging from 70 to 115 m, with the deepest depths in the southwestern portions of the study area (Figure 3g). In 2020, MLD varied from 24 to 130 m, with the shallowest depths observed in the coastal waters, most notably near Haida Gwaii, where the lowest SSS were observed. Oceanic MLDs in 2020 were deeper than those in comparable locations in 2019, resulting in a higher annual mean despite the inclusion of the more stratified coastal waters (Figure 3h). In contrast to MLD, DO was higher in 2019 than in 2020 with near uniform concentrations across the oceanic region, varying from 6.73 to 7.11 ml/L, and showing elevated levels in conjunction with the low sigma-t feature (Figure 3i). In 2020, surface DO ranged from 6.08 to 6.83 ml/L and displayed a slight longitudinal trend, with lower values toward Vancouver Island and increasing toward the subarctic water mass (Figure 3j).

Spatially, in both years, surface inorganic nutrients exhibited latitudinal and longitudinal gradients similar to SST and SSS (Figure 3), with higher concentrations in the subarctic water mass. Between years (Figures 4a–4f), 2019 generally showed higher nutrients than 2020 (Table 1), with high nutrients spanning much of the subarctic water mass. In 2020, high nutrient concentrations were observed in the low MLD/SSS continental shelf waters near Haida Gwaii and low concentrations in the subtropical water mass off Vancouver Island (Figures 4b, 4d, and 4f). Additionally, in 2020 an elevated DIP feature was observed near 50° N (Figure 4d).

3.2. EOF-Based Phytoplankton Community Composition Retrieval

3.2.1. Algorithm Evaluation and Cross-Validation

The regression model trained using the matchup data set showed the best performance for Hapto/Pelago/Cyano and Diatoms/Dino/GA groups (e.g., $R^2 = 0.45$, 0.42, respectively; $p < 0.0001$), followed by TChla ($R^2 = 0.27$) and Crypto ($R^2 = 0.24$). The MAE for all phytoplankton groups was generally low, ranging from 0.01 to 0.04 mg m^{-3}. Overall, BIAS and MDPD varied from 2.33% to 26.37% and 12.42%–43.49%, respectively

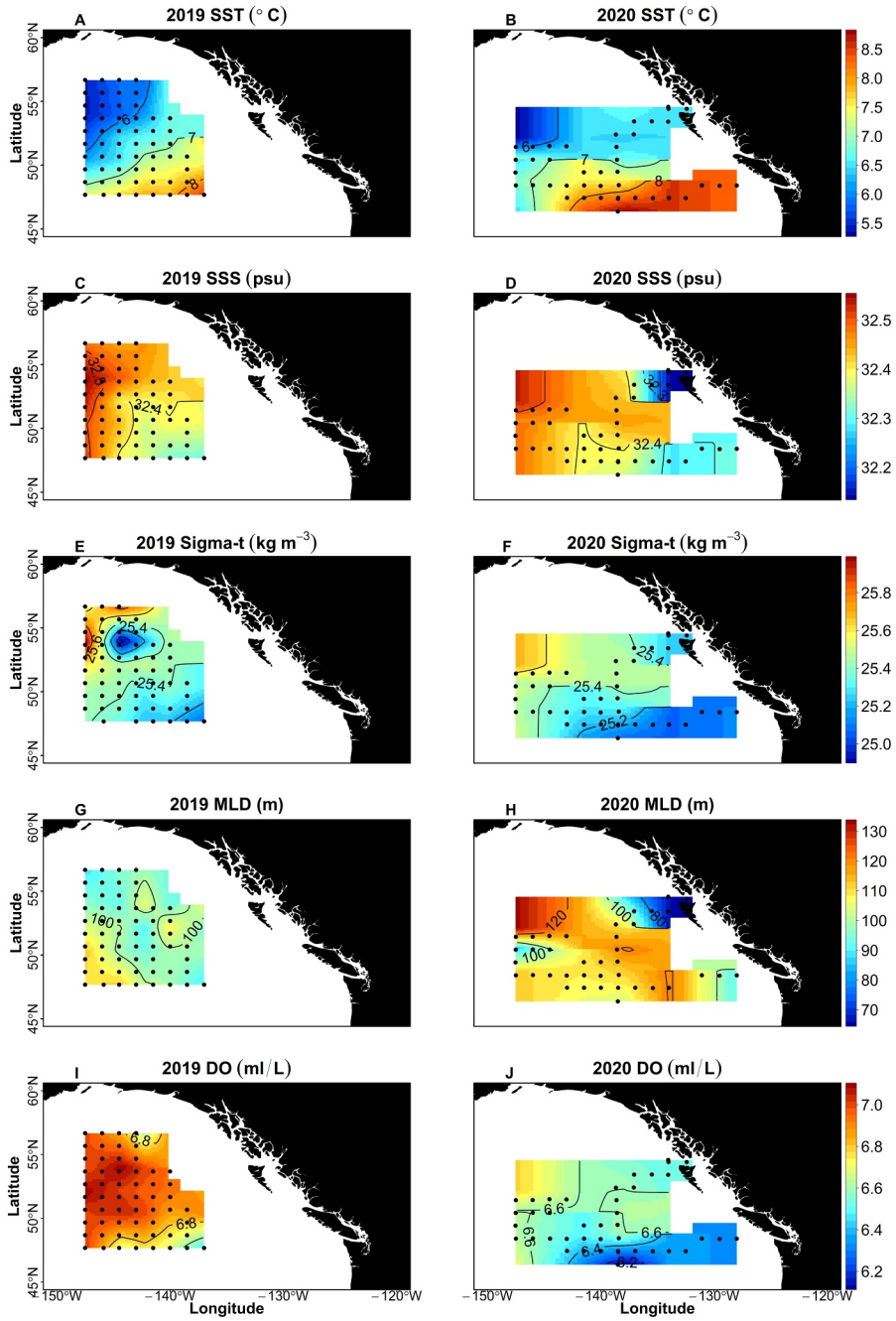

Figure 3. Distribution of surface water properties of the subarctic northeast Pacific for 2019 and 2020: (a, b) sea surface temperature (SST; °C), (c, d) sea surface salinity (SSS; PSU), (e, f) potential density (sigma-t; kg m^{-3}), (g, h) mixed layer depth (MLD; m), and (i, j) surface dissolved oxygen (DO; ml/L). Black points represent individual sample observations. The 2019 data set covers from February 18 to March 21, whereas the 2020 spans from March 5 to April 5.

(Table 2), with the highest positive BIAS (i.e., overestimation) and MDPD obtained for Crypto (26.37%; 43.49%, respectively). In contrast, TChla exhibited the lowest BIAS and MDPD values (2.33% and 12.42%, respectively). A cross-validation procedure was performed to assess further the fitted regression model's robustness, yielding results comparable to the full-fit statistics (Table 2). It is worth noting that a significant R^2_{CV} value of 0.25 was obtained for the Diatom/Dino/GA, followed by the Hapto/Pelago/Cyano group (0.24), whereas the lowest R^2_{CV} were noted for Crypto (0.21) and TChla (0.23). Consistent with the full-fit statistics, the best MAEcv (0.01 mg m^{-3}) and MDPDcv (13.85%) were achieved for TChla concentrations, whereas Crypto recorded a high

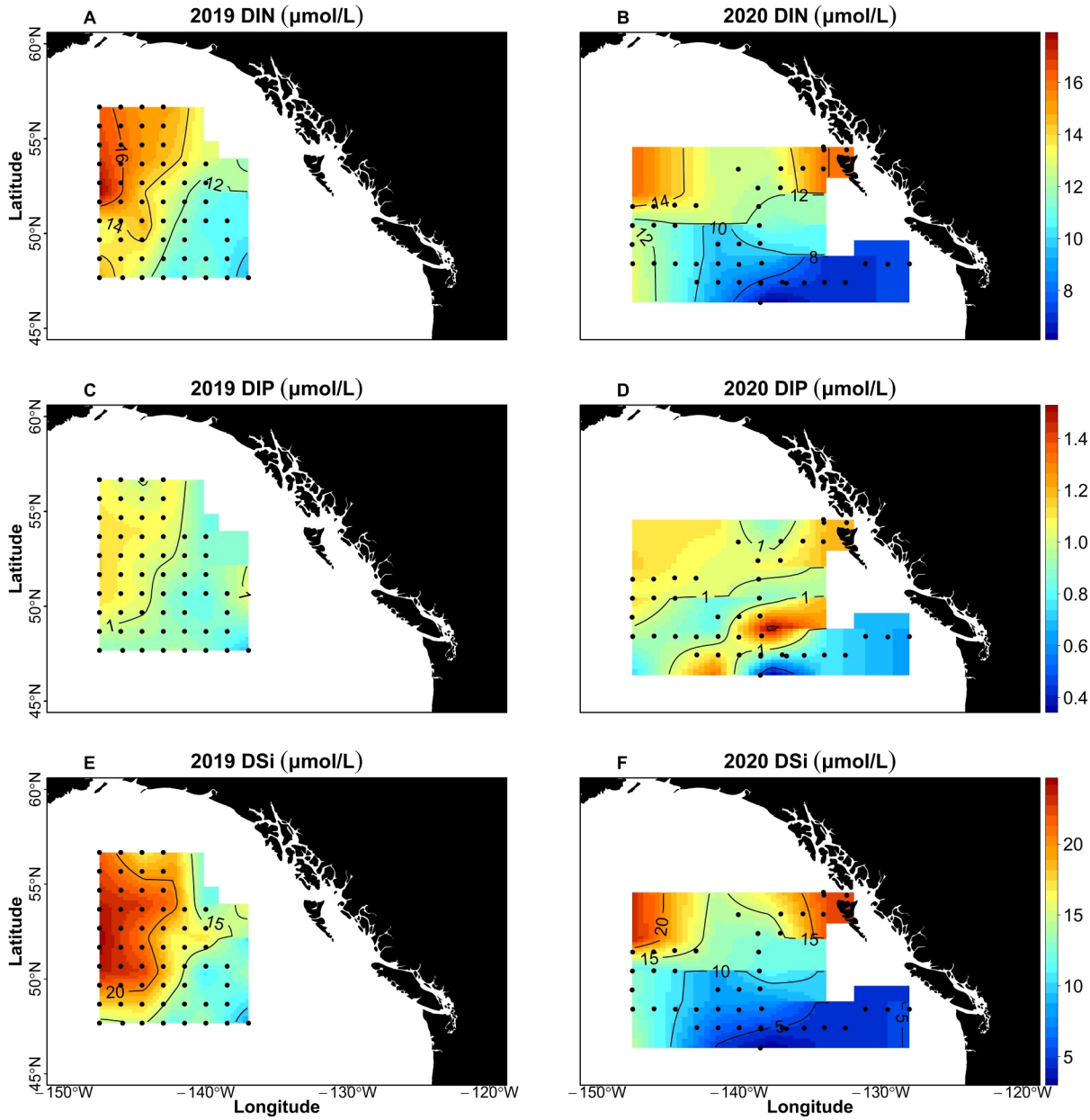

Figure 4. Spatial distribution of dissolved inorganic nutrients in the surface waters of the subarctic northeast Pacific for 2019 and 2020: (a, b) dissolved inorganic nitrogen (DIN; µmol/L), (c, d) dissolved inorganic phosphate (DIP; µmol/L), and (e, f) dissolved inorganic silicate (DSi; µmol/L). Black points represent individual sample observations. The 2019 data set covers from February 18 to March 21, whereas the 2020 spans from March 5 to April 5.

MDPDcv of 44.74%. Details on the discussion of the performance of the regression model are provided in the Supporting Information S1 (Text S1 in Supporting Information S1).

3.2.2. Independent Validation

As a second level of independent validation, we conducted a semi-quantitative comparison of the OLCI retrievals against Line-P CHEMTAX-derived phytoplankton composition data to demonstrate the similar dynamic range of each phytoplankton group from both methods (Table 3; Figure S4 in Supporting Information S1). Among the considered groups, Hapto/Pelago/Cyano demonstrated a strong agreement between data sets (R^2 = 0.32, MAE = 0.03 mg m^{-3}, BIAS = 8.5%, MDPD = 9.9%, $p < 0.001$; Table 3), followed by cryptophytes (R^2 = 0.27, MAE = 0.03 mg m^{-3}, BIAS = 26.37%, MDPD = 43.49%, $p < 0.05$; Table 3). In contrast, no agreement was

Table 1
Distribution of Physicochemical Properties, CHEMTAX-Derived Phytoplankton Community Composition, and Nutrient Concentrations During 2019 and 2020

Variables	Years	
	2019	2020
SST (°C)	[5.04–8.20]	[5.25–9.31]
	6.57 (0.75)	**7.25** (0.94)
Salinity (psu)	[32.34–32.63]	[32.14–32.54]
	32.43 (0.06)	**32.37** (0.21)
Potential density (kg m^{-3})	[24.29–25.81]	[24.50–25.70]
	32.43 (0.06)	**25.31** (0.21)
MLD (m)	[70–115]	[24–130]
	98 (10)	104 (22)
DO (ml/L)	[6.73–7.11]	[6.08–6.83]
	6.97 (0.10)	**6.49** (0.15)
NO_3+NO_2 (µmol/L)	[9.15–18.71]	[4.77–20.65]
	13.53 (2.38)	**10.90** (3.38)
PO_4 (µmol/L)	[0.77–1.31]	[0.56–2.22]
	1.00 (0.12)	**0.98** (0.31)
SiO_4 (µmol/L)	[6.67–27.96]	[2.70–32.59]
	18.64 (4.78)	**11.06** (6.82)
Cyano (mg m^{-3})	[0.01–0.04]	[0–0.01]
	0.02 (0.01)	**0.01** (0.005)
Hapto (mg m^{-3})	[0.06–0.21]	[0.06–0.20]
	0.14 (0.04)	**0.10** (0.04)
Pelago (mg m^{-3})	[0.02–0.09]	[0.02–0.06]
	0.05 (0.02)	**0.04** (0.01)
Chlor (mg m^{-3})	[0–0.08]	[0–0.09]
	0.01 (0.01)	**0.03** (0.04)
Prasino (mg m^{-3})	[0.01–0.07]	[0.01–0.15]
	0.04 (0.01)	**0.08** (0.03)
Crypto (mg m^{-3})	[0.01–0.11]	[0–0.06]
	0.03 (0.02)	**0.03** (0.02)
Dino (mg m^{-3})	[0.01–0.05]	[0.04–0.11]
	0.03 (0.02)	**0.07** (0.02)
Diatoms (mg m^{-3})	[0–0.04]	[0–0.14]
	0.01 (0.01)	**0.03** (0.04)
TChla (mg m^{-3})	[0.17–0.50]	[0.21–0.52]
	0.35 (0.07)	**0.37** (0.12)

Note. Minimum and maximum values are shown in square brackets, average in bold and standard deviation (±SD) in parenthesis. The 2019 data set covers from February 18 to March 21, whereas the 2020 spans from March 5 to April 5.

observed for Diatoms/Dino/GA (R^2 = 0, MAE = 0.02 mg m^{-3}, BIAS = −1.35%, MDPD = 14.5%; Table 3), although their spatial distribution patterns aligned well with our CHEMTAX-derived output (see Figure S4 in Supporting Information S1) and were consistent with patterns reported in the literature. Finally, TChla showed the best agreement between OLCI and Line-P data (R^2 = 0.53; MAE = 0.01 mg m^{-3}, BIAS = −17.39%, MDPD = 21.06%, $p < 0.001$; Table 3).

Table 2
Full-Fit and Cross-Validation Statistics Derived From the EOF Analysis Performed on the Matchup Between OLCI Rrs(λ) and the CHEMTAX-Derived Phytoplankton Community Composition

	N	R^2	MAE (mg m^{-3})	BIAS (%)	MDPD (%)	R^2cv	MAEcv	MDPDcv	p-value
Hapto/Pelago/Cyano	61	0.45	0.03	5.17	16.85	0.24	0.05	18.20	0.3710^{-8}
Diatom/Dino/GA	61	0.42	0.02	5.34	20.51	0.25	0.03	23.93	0.1410^{-8}
Crypto	59	0.24	0.01	26.37	43.49	0.21	0.01	44.74	0.7910^{-5}
TChla	61	0.27	0.04	2.33	12.42	0.23	0.01	13.85	0.1810^{-5}

Note. N: Number of samples; R^2: Coefficient of determination; MAE: Mean absolute error (mg m^{-3}); BIAS: Mean percentage bias between predicted and observed concentrations (%); MDPD: Median percentage difference (%); R^2cv: Cross-validated coefficient of determination; MAEcv: Cross-validated mean absolute error (mg m^{-3}); MDPDcv: Cross-validated median percentage difference (%); p-value: Probability value for significance testing.

3.2.3. Spatio-Temporal Distribution of Sentinel-3 OLCI-Derived Phytoplankton Groups

The spatial distribution of TChla values across the mostly open ocean waters of the SNEP during 2019 and 2020 are shown in Figure 5. In 2019, TChla concentrations were stable across the four weekly composites (0.35 ± 0.07 mg m^{-3}), with a subtle increase in TChla levels discernible north of 55°N. In 2020, TChla concentrations were similarly consistent across the four weekly composites (0.32 ± 0.06 mg m^{-3}), with a notable increase in the concentration found toward the continental shelf near Haida Gwaii. Figures 6 and 7 show the spatial distribution of Hapto/Pelago/Cyano, Diatoms/Dino/GA, and Crypto during 2019 and 2020, respectively. In 2019, all phytoplankton groups exhibited low Chl a concentrations and a relatively homogeneous distribution across offshore waters, with only subtle variations observed among the weekly composites (Figure 6). Consistent with the Line-P CHEMTAX data, the highest average contributions in 2019 were from Hapto/Pelago/Cyano, followed by Diatoms/Dino/GA and then Crypto (0.21, 0.12, 0.03 mg m^{-3}, respectively). Similar to 2019, a spatially homogeneous distribution was found for all groups in the open ocean in 2020 (Figure 7). However, a patch of increased contributions was recorded for Diatoms/Dino/GA on the continental shelf off of Haida Gwaii that was matched by decreased Hapto/Pelago/Cyano contributions. The highest average Chl a concentration from 2020 was by Hapto/Pelago/Cyano, followed by Diatoms/Dino/GA and then Crypto (0.17, 0.12, 0.02 mg m^{-3}, respectively).

Figure 8 illustrates the OLCI-derived phytoplankton group Chl a concentrations and TChla extracted from latitudinal transects in 2019 and longitudinal transects in 2020. These plots highlight more subtle trends not easily viewable in Figures 5–7. Across all groups, including TChla, concentrations remained relatively invariant within the HNLC region. However, elevated Chl a concentrations were observed in 2019, particularly for cryptophytes, Diatoms/Dino/GA, and TChla, toward the northern extents of the study region. In contrast, the 2020 data revealed

Table 3
Statistical Metrics Obtained From the Independent Validation Comparing Phytoplankton Group Chl a Concentrations Derived From the 2019 and 2020 OLCI Weekly Composites Along the Line-P Transect With Corresponding In Situ CHEMTAX-Derived Values

	N	R^2	MAE (mg m^{-3})	BIAS (%)	MDPD (%)	p-value
Hapto/Pelago/Cyano	29	0.32	0.03	8.5	9.9	$p < 0.001$
Crypto	29	0.27	0.03	26.37	43.49	$p < 0.05$
Diatom/Dino/GA	29	0	0.02	−1.35	14.5	$p > 0.1$
TChla	29	0.53	0.01	−17.39	21.06	$p < 0.001$

Note. The utilized Line-P stations were limited to those from HNLC waters extending from the southwest of Vancouver Island to Ocean Station Papa (OSP) (see Figure 1). Coastal stations (i.e., P1 and P2) were excluded due to their high spatial and temporal variability. In 2019, OLCI-derived phytoplankton groups were retrieved between February 18 and March 21, whereas the corresponding Line-P data were collected between February 6 and 12. Similarly, in 2020, OLCI retrievals occurred from March 5 to April 5, with Line-P data collected primarily between February 10 and 16. N: Number of samples; R^2: Coefficient of determination; MAE: Mean absolute error (mg m^{-3}); BIAS: Mean percentage bias between predicted and observed concentrations (%); MDPD: Median percentage difference (%); p-value: Probability value for significance testing; TChla: total Chlorophyll-a concentration (mg m^{-3}).

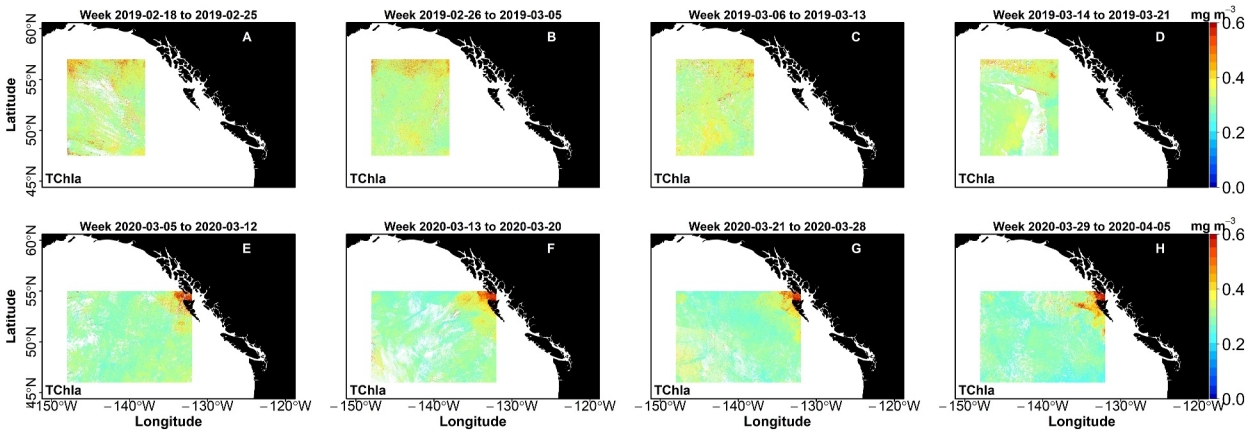

Figure 5. Spatial distribution of TChla concentration retrieved over the subarctic northeast Pacific from the 2019 and 2020 weekly composite OLCI imagery. The spatial extent of the TChla was limited to the coverage of the matchup data set. Extending the algorithm's application to the region outside the matchup area may result in unreliable retrievals; therefore, the spatial extension was constrained to match the coverage of the matchup data set from 2019 to 2020. White regions on the map represent clouds. This is the same for this figure and Figures 6 and 7. The 2019 data set covers from February 18 to March 21, and the 2020 data set covers from March 5 to April 5.

increased Chl a concentrations of Diatoms/Dino/GA and TChla along the Haida Gwaii shelf, accompanied by corresponding decreases in Hapto/Pelago/Cyano.

3.3. CHEMTAX-Derived Phytoplankton Community Composition

The CHEMTAX-derived phytoplankton community compositions for 2019 and 2020 are shown in Figure 9. Overall, low surface TChla (Figure 9c) concentrations were observed throughout the study period, ranging from 0.17 to 0.52 mg m^{-3}, with an average of 0.35 mg m^{-3}, and a diverse phytoplankton community was present across the region. In 2019, haptophytes were the dominant group (0.16 ± 0.04 mg m^{-3}, 47 ± 6%; Figure 9d), followed by pelagophytes (0.06 ± 0.02 mg m^{-3}, 17 ± 3%; Figure 9e) and green algae (0.05 ± 0.01 mg m^{-3}, 15 ± 6%). Within the green algae (Figures 9f and 9g) community, prasinophytes were the predominant group (0.04 ± 0.01 mg m^{-3},

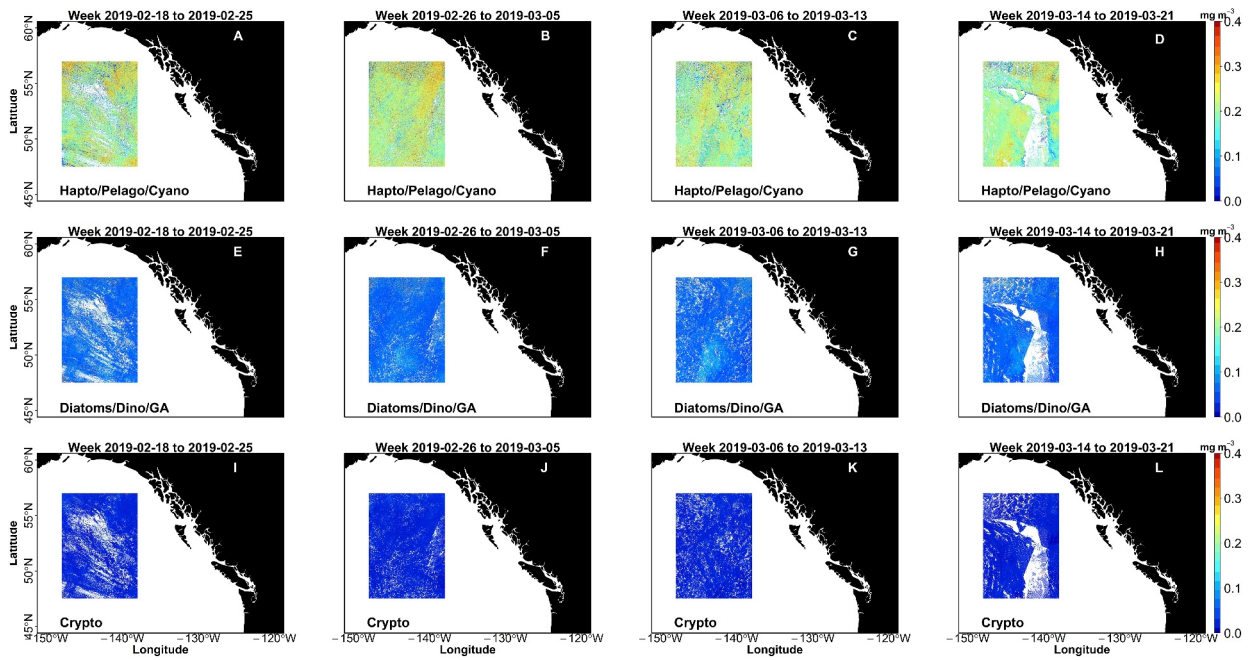

Figure 6. Spatial distribution of Hapto/Pelago/Cyano, Diatoms/Dino/GA, and cryptophytes Chl a concentration retrieved over the subarctic northeast Pacific from the 2019 weekly binned OLCI imagery. This data set spans from February 18 to March 21.

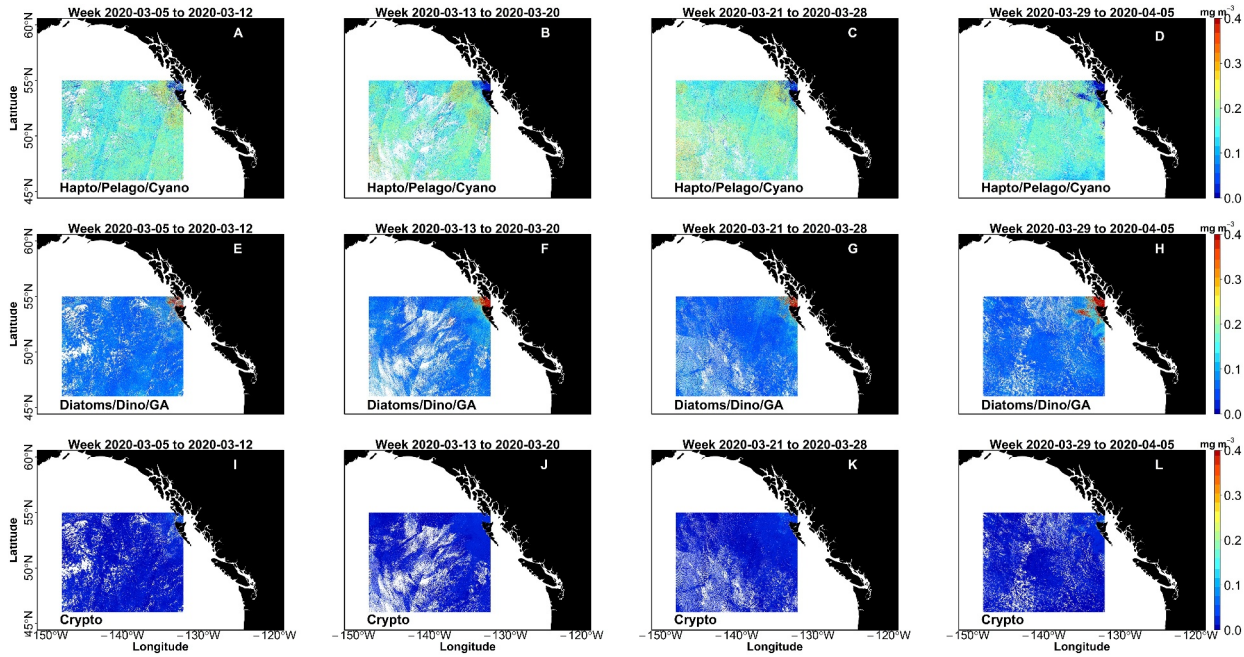

Figure 7. Spatial distribution of Hapto/Pelago/Cyano, Diatoms/Dino/GA, and cryptophytes Chl a concentration retrieved over the subarctic northeast Pacific from the 2020 weekly binned OLCI imagery. This data set spans from March 5 to April 5.

11 ± 3%). Diatoms, dinoflagellates, cryptophytes, and cyanobacteria were the less abundant groups throughout the region (2 ± 3%, 6 ± 1%, 6 ± 3%, and 6 ± 3%, respectively). In 2019, the community compositions were very similar throughout the study region, except for increased contributions by cryptophytes in the northern portion of the subarctic water mass (Figure 9j, stations 18–24), which is consistent with the OLCI results (Figure 8c).

In 2020, phytoplankton community composition data were primarily limited to the outer continental shelf and Dixon Entrance (see Figure 9c), with only a few stations located in the open ocean, which makes it challenging to compare offshore regions between both years. Interestingly, samples from Dixon Entrance showed relatively high TChla levels (0.51 mg m^{-3}), with no contribution from haptophytes and a notable diatom contribution (31%). Consistent with this finding, OLCI output also showed a similar distribution pattern for the merged Hapto/Pelago/Cyano and Diatom/Dino/GA groups on the continental shelf, indicating longitudinal differences between offshore and coastal regions. In contrast, stations on the outer continental shelf showed moderate TChla concentrations (avg 0.43 mg m^{-3}), with the green algae group contributing the most (31%), followed by haptophytes (27%). Finally, a few offshore stations sampled in 2020 showed lower TChla levels (avg 0.24 mg m^{-3}), with haptophytes as the dominant group (31%), followed by the green algae group (25%), which is somewhat comparable to the offshore samples from 2019.

3.4. Environmental Drivers

Redundancy analysis using the eight CHEMTAX-derived phytoplankton group contributions and matching environmental variables had an $r^2 = 0.42$ ($p = 0.001$) with RDA1 explaining 36% of the variance ($p = 0.001$) and RDA2 6% of the variance ($p = 0.01$) (Figure 10). The forward-selected significant variables were SSS (28% of variance, $p = 0.0001$), MLD (6%, $p = 0.01$), DSi (5%, $p = 0.002$), and SST (3%, $p = 0.01$). The RDA triplot (Scaling 2) showed large differences between years representing longitudinal open ocean-coastal variability along RDA1, with 2019 (dominantly open ocean samples) having higher contributions by haptophytes, prasinophytes, cyanobacteria, and pelagophytes; and 2020 (mostly shelf/coastal samples) having higher contributions by diatoms, dinoflagellates, and chlorophytes. Furthermore, the 2019 open ocean groups were strongly positively correlated with MLD and SSS, whereas the 2020 shelf/coastal groups were negatively correlated with these drivers and groups. RDA2 was largely driven by latitudinal differences, with the subarctic water mass samples showing higher DSi and cryptophyte contributions and an inverse correlation with SST and the more subtropical

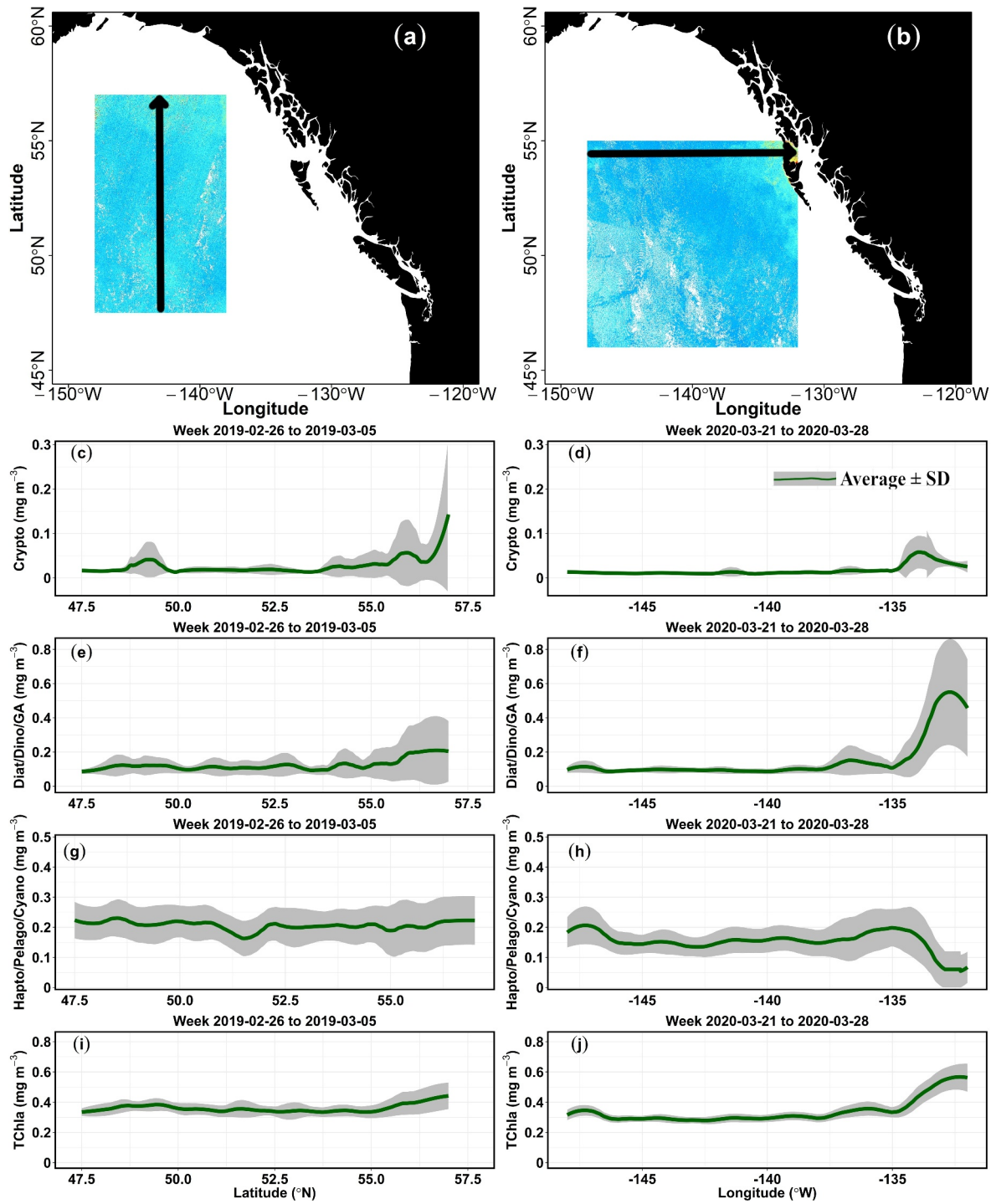

Figure 8. Latitudinal (2019) and longitudinal (2020) transects of OLCI-derived surface Chl a concentration for cryptophytes, Hapto/Pelago/Cyano, Diatoms/Dino/GA, and TChla. Data were extracted from the least cloud-affected composites for 2019 and 2020. For 2019, the selected period was February 26 to March 5, whereas for 2020, it was March 21 to 28. The Chl a concentrations were extracted over a 5x5-pixel window, with gray-shaded regions representing the standard deviation (±SD). Panels (a, b) display the TChla (mg m^{-3}) map as an example with overlaid latitudinal and longitudinal transect lines, illustrating the location used to extract transects for each phytoplankton group in 2019 and 2020, respectively. Color gradients represent the range of TChla concentrations across these transects. Panels (c, e, g, and i) show the 2019 latitudinal distribution of surface Chl a concentrations for the main phytoplankton groups, including TChla, from February 26 to March 5. Panels (d, f, h, and j) display the 2020 longitudinal distribution for the same groups from March 21 to 28.

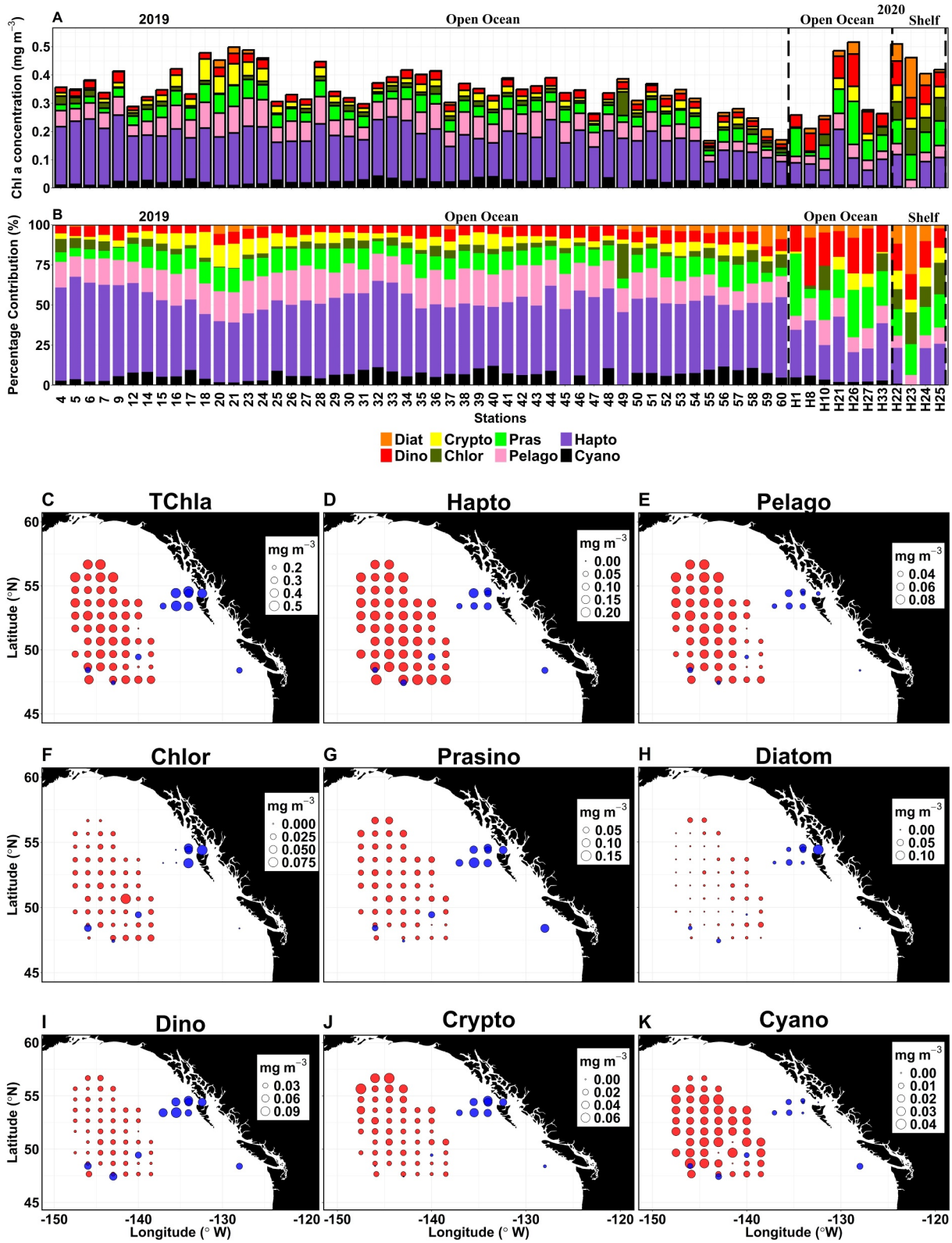

Figure 9. Spatial distribution of CHEMTAX-derived phytoplankton community composition in the surface waters of the subarctic northeast Pacific for 2019 and 2020. (a) Chl a concentration of cyanobacteria, cryptophytes, diatoms, dinoflagellates, haptophytes, pelagophytes, chlorophytes, prasinophytes, and TChla. (b) Percentage contribution of each group. (c–k) spatial distribution of each of these groups. The red and blue circles represent 2019 and 2020, respectively. The 2019 data set covers from February 18 to March 21, whereas the 2020 spans from March 5 to April 5.

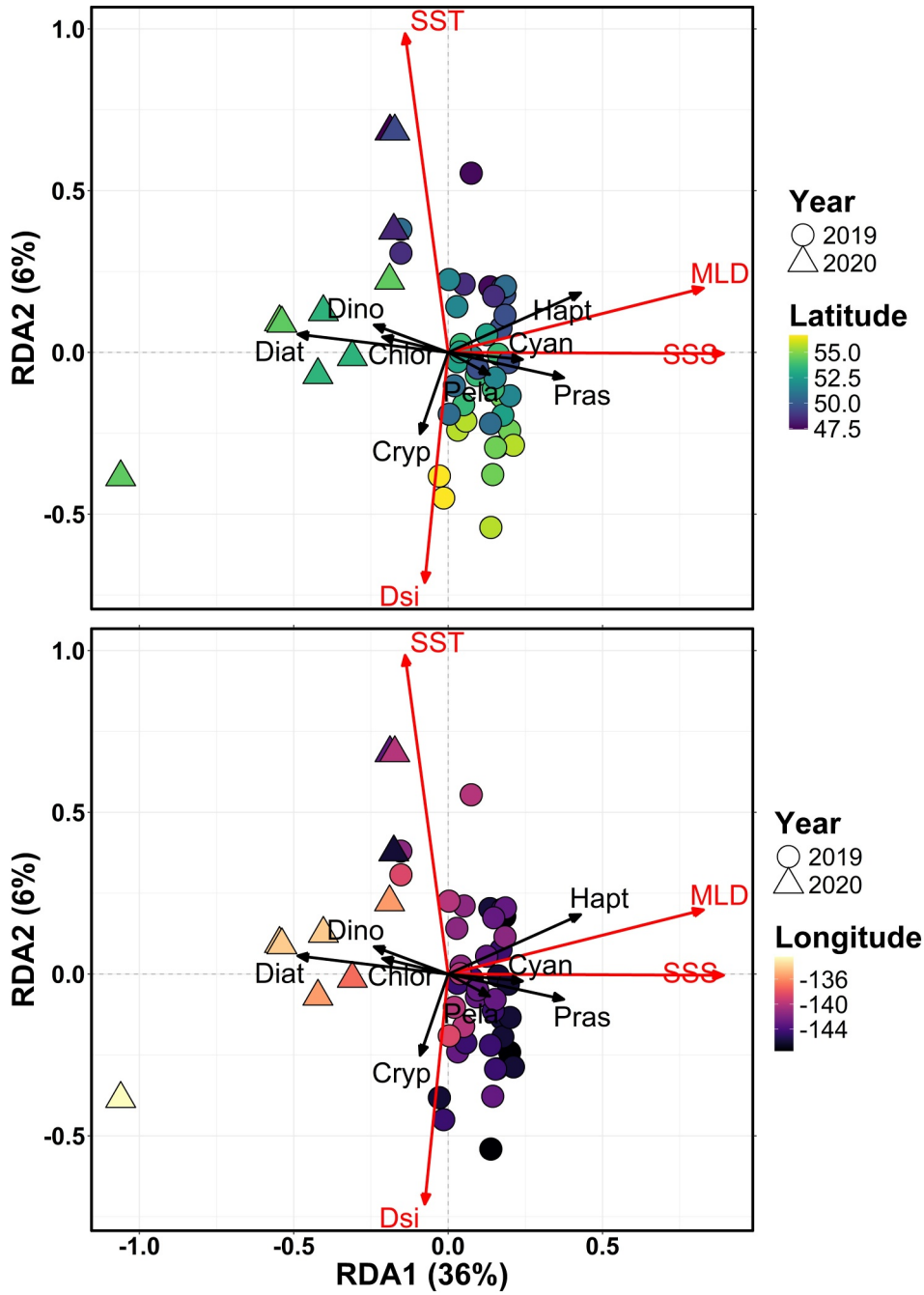

Figure 10. The redundancy analysis triplot (Hellinger transformation, scaling 2) illustrates the relationship between response and explanatory variables. The red arrows indicate statistically significant explanatory variables, sea surface temperature (SST), sea surface salinity (SSS), mixed layer depth (MLD), and dissolved silicate (DSi), and the black arrows show the CHEMTAX-derived phytoplankton community composition. The shape of each point represents the collection year, with circles for 2019 and triangles for 2020. The color of the points represents the latitude (a) and longitude (b) of the sample collection location. The global model was significant with $p < 0.001$, and the explanatory variables explained 42% of the constrained variance in the CHEMTAX-derived phytoplankton community composition. Scaling 2 was used for the triplot with the angle between arrows, both response and explanatory, indicating the linear correlation between the variables. For example, an angle of 90° shows no correlation, whereas an angle less than 90° indicates a positive correlation, and an angle greater than 90° indicates a negative correlation.

water mass samples. Results of RDA analysis between environmental drivers and the OLCI-derived phytoplankton groups found no significant forward-selected variables; therefore, they were not presented.

4. Discussion

This research used CHEMTAX-derived and OLCI-derived phytoplankton composition data to provide an overview of the spatio-temporal distribution of phytoplankton groups and their potential environmental drivers in the SNEP, limited to winter conditions in 2019 and 2020. The data set showed distinct water masses in the region with the 7°C isotherm demarcating the boundary between the subarctic water mass to the northwest and the subtropical water mass to the southeast (see Figure 5; Pakhomov et al., 2022). Additionally, the continental shelf region off Haida Gwaii, sampled only in 2020, was dominated by the ACC and showed coastal influences. Broadly, all physical and chemical variables tended to follow these regionally distinct water masses. Both CHEMTAX and OLCI-derived phytoplankton community composition data showed a largely homogeneous distribution dominated by small flagellates such as haptophytes, green algae, and pelagophytes in the open ocean waters. However, a few exceptions to this homogeneity were observed, including increased 2019 cryptophyte contributions in the northern extent of the study area where winter phytoplankton communities are generally homogeneous (Ross & Peña, 2022) and increased 2020 TChla and diatom contributions observed on the shelf waters. The following sections provide a discussion of the major findings of this study.

4.1. Phytoplankton Community Composition and Their Response to the Environmental Drivers

Spatio-temporally, our CHEMTAX and OLCI retrievals generally align with previous findings on phytoplankton community composition in the SNEP region. Specifically, in the offshore regions under winter conditions, we observed low and invariant TChla with communities dominated by small-sized (<10 μm) flagellates such as haptophytes, followed by pelagophytes and green algae and low diatom contributions (Booth et al., 1993; Fujiki et al., 2009; Peña & Nemcek, 2021; Peña et al., 2019). Peña et al. (2019) and Peña and Nemcek (2021) have shown that haptophytes often constitute >50% of the total phytoplankton community during winter conditions in the Alaskan Gyre waters. In addition, Fujiki et al. (2009) showed that green algae contributed up to 30% to the total phytoplankton community throughout the Alaska Gyre, and while ubiquitous, pelagophytes contributed <20% to the total phytoplankton biomass during the winter of 2019 and 2020 (Peña & Nemcek, 2021). Similarly, recent studies using comparable EOF-based methods agree well with our observations, showing comparable SNEP trends for haptophytes and green algae obtained from 10 years (2002–2012) (Xi et al., 2020) and 20 years (2002–2022) (Konik et al., 2024) of GlobColor merged satellite imagery. In addition to the offshore trends, our CHEMTAX and satellite observations showed increased TChla and diatom contributions and decreased haptophyte contributions toward the Haida Gwaii Shelf, which is expected for more coastal waters (Nemcek et al., 2023; Waite & Mueter, 2013). Of interest, and unique to this study, was the notable increases in cryptophyte contributions toward the northern GoA. Below, we discuss various environmental drivers that may have driven these observations.

The observed trend of low phytoplankton biomass and haptophyte dominance in the Alaska Gyre offshore waters was likely driven by the combination of multiple factors. Although BFe was not measured here, previous studies have shown phytoplankton biomass and species composition in Alaska Gyre are largely dependent on BFe availability (e.g., Harrison et al., 2004; Marchetti et al., 2006; Martin et al., 1991; Nishioka et al., 2021; Zhang et al., 2021), with iron limitation promoting the occurrence of small flagellates such as haptophytes (Endo et al., 2018; Fujiki et al., 2009; Peña et al., 2019) throughout the year (Peña et al., 2019; Yang et al., 2018; Zhang et al., 2021). Evidence of this limitation and its influence on phytoplankton communities has been demonstrated during the non-light limiting growing season by aerial BFe deposition events driving increased diatom biomass (Bishop et al., 2002; Boyd et al., 1998; Hamme et al., 2010; Marchetti et al., 2006; Nishioka et al., 2021). Yet, our results from the winter months were likely more influenced by deep mixing and light limitation, which is supported by the observed deep MLDs (MLD = 123 m) and positive RDA based correlations between haptophytes and MLD and SSS. Under these conditions, surface phytoplankton biomass is diluted, and strong light limitation is experienced as winter light levels are already low and cells are mixed deeper than the euphotic depth, further limiting light exposure (Maldonado et al., 1999; Strom et al., 2010). These conditions promote small flagellates that have competitive advantages over large diatoms as a result of their small pigment packaging effect, making them efficient light harvesters (Alexander et al., 2015; Endo et al., 2018; Gregg & Casey, 2007; Marañón et al., 2012; Margalef, 1995). Contrastingly, we observed an increase in phytoplankton biomass and diatom

contributions in the more coastal waters, providing further evidence that a combination of the above factors promoted small phytoflagellate dominance in the offshore waters.

The shelf and coastal waters off of Haida Gwaii showed increased phytoplankton biomass driven by higher diatom contributions, which were associated with both reduced SSS and MLDs. In these waters, coastal influences likely provided the necessary BFe for diatom growth (Cullen et al., 2009; Johnson et al., 2005; Strom et al., 2016; Whitney et al., 2005). Furthermore, the observed decreased SSS and MLD would have increased stratification, limiting surface phytoplankton biomass dilution and allowing cells to remain within the photic zone for longer periods, increasing light exposure and promoting growth (Henson, 2007). Importantly, seasonal increases in freshwater-driven stratification have been shown to be a prominent driver of spring diatom blooms in the shelf and coastal GoA (Brickley & Thomas, 2004; Childers et al., 2005) with TChla often >3 mg m^{-3} (e.g., Brickley & Thomas, 2004; Giannini et al., 2021; Jackson et al., 2015; Marchese et al., 2022; Nemcek et al., 2023; Ribalet et al., 2010; Strom et al., 2016; Vishnu et al., 2022; Waite & Mueter, 2013). In comparison, our winter/start of the spring observations showed considerably lower (≤0.14 mg m^{-3}) diatom contributions, likely as a result of light availability still not being sufficient to trigger the annual bloom (Fiechter & Moore, 2009). In these shelf waters, small flagellates such as haptophytes were still important (see Figure 7), which is common during winter conditions in the coastal northeast Pacific region and likely highlights the continuation of winter light limitation and the adaptability of species within these groups to a broad range of conditions (Del Bel Belluz et al., 2021; Endo et al., 2018).

Unique to our study was the observed increase in cryptophyte abundance at the northern extents of the study area in 2019, which was observed with both the in situ CHEMTAX-derived data and the OLCI data (Figures 8c and 9j). This observation may have been a result of several interconnecting factors, including SST, MLD, and coastal water influences introduced via eddies and the transition zone with the ACC. Statistically, our RDA analysis showed increased DSi and reduced SST associated with this increase in cryptophyte contributions. Yet, nutrients were high and non-limiting across the study area, indicating that they likely did not play a role in the increased cryptophyte contributions. Rather, the RDA-based correlations were likely driven by similar gradients with the study area crossing the transition into the North Pacific Drift Current water mass, driving the observed increases in nutrients and reduced temperatures moving northward where cryptophyte contributions were also elevated (Figure 3a; Thomson & Krassovski, 2010). Despite the gradient-driven negative correlation with SST, winter marine heatwave conditions were present in 2019, with the highest temperature anomalies observed in the northern GoA, and were associated with higher than normal winter stratification and lower MLDs (Amaya et al., 2020; Pakhomov et al., 2022; Ross & Peña, 2022). Lower MLDs were observed in our data in 2019 being approximately 88 m, which is shallow compared to the oceanic regions studied in 2020. It is possible that these factors worked to promote the observed increases in cryptophyte contributions as increased temperatures have been linked to higher cryptophyte biomass in Antarctic waters (Mendes et al., 2018), and reduced MLDs would have worked to increase light exposure and minimize dilution of surface phytoplankton (Mendes et al., 2013; Pan et al., 2020). Similar to haptophytes, cryptophytes are efficient light harvesters, giving them a competitive advantage in highly fluctuating light conditions (Mendes et al., 2023). In addition to these conditions, two large eddies (Sitka and Yakutat eddies) were present in winter 2019 directly north of our study area extent (Pakhomov et al., 2022; Ross & Peña, 2022). These types of eddies have been shown to enhance offshore transport of coastal iron-rich waters and potentially more coastal communities into the GoA (Crawford, 2005; Lippiat et al., 2010). Increased nano-plankton and cryptophytes have been observed in both the outer rings of eddies (Damini et al., 2023) and within transition zones between the Alaska Gyre and coastal waters off of the Aleutian Islands (Juranek et al., 2020). Although the drivers of this observation remain elusive, we hypothesize that the combination of winter marine heatwave conditions and their interaction with eddies and/or the location of the transition zone worked to enhance cryptophyte biomass in the oceanic northern GoA, which typically experience homogenous phytoplankton communities comparable to the rest of the region.

An important contrast to the above hypothesis was that eddies were also present in 2020, but the OLCI-derived phytoplankton groups (Figure 7) did not show a notable trend. One consideration is that in 2020, the study area did not extend northward into the area where the increased cryptophyte contributions were observed in 2019. Therefore, we are unclear as to whether these increased contributions continued into 2020. This is a shortcoming, as comparable observations in the northern region in 2020 would have helped to define the drivers of the increased cryptophyte contributions in 2019. Yet, in 2020, the eddies were situated in more southern regions that were covered by satellite imagery and did not show comparable changes in phytoplankton community composition to

2019. Typically, regional eddy-driven changes in phytoplankton community compositions across the SNEP primarily occur under non-light limiting growing season conditions with minimal differences observed in winter (Crawford, 2005; Okkonen et al., 2003). Importantly, unlike 2019, 2020 did not show winter marine heatwave conditions, and in the offshore waters, MLDs were considerably deeper (130 m) than those observed in 2019 (some areas were as shallow as approximately 90 m). Consequently, despite both years showing eddy influences, 2020 displayed more "winter-like" offshore conditions likely driving more phytoplankton dilution and light limitation, dampening any eddy-driven influence.

Beyond the role of physicochemical drivers on phytoplankton community composition, top-down control from zooplankton grazing can inhibit regional phytoplankton biomass accumulation (Landry et al., 1993; Miller, 1993) and shape the community composition via selective grazing (Landry et al., 1993; Strom & Welschmeyer, 1991). These top-down controls were not addressed in this study but are important considerations for explaining the observed trends. In both studied years (i.e., 2019 and 2020), the highest zooplankton abundances were observed in the southern portions of the study area (Pakhomov et al., 2022) and generally coincided with reduced phytoplankton biomass. However, these authors showed that in 2020 zooplankton abundance was notably higher than in 2019 (~650 and ~400 ind.m^{-3}, respectively), with elevated abundances coinciding with the reduced phytoplankton biomass and reduced haptophyte and pelagophyte contributions when compared to 2019, as shown by our results. Additional studies combining high spatio-temporal phytoplankton composition data derived from satellite imagery with zooplankton data could provide further insights into the role of top-down control in shaping the phytoplankton community composition.

4.2. Limitations in Our In Situ and Satellite Data

Multiple sources of uncertainty are associated with in situ HPLC pigment/CHEMTAX analysis and OLCI methods for deriving phytoplankton community composition in ocean waters. Regarding HPLC phytoplankton pigment measurements, differences in analytical methods used between studies have been shown to introduce uncertainties of up to 7% for TChla and 21% for accessory pigments (Claustre et al., 2004). These uncertainties are essential to consider when comparing the methods used in this study with other data sets and regions where HPLC pigment data were analyzed using alternative approaches. In this study, HPLC pigment samples were analyzed at the University of South Carolina's Baruch Institute (https://phytoninja.com/lab-protocols/) following the method outlined by Pinckney (2010). To evaluate analytical precision, duplicates were collected and analyzed for 20% of the samples (n = 11) from 2019, which resulted in a coefficient of variation (CV) below 20%, indicating the analytical precision of the method and instrument used.

Uncertainty can also be introduced by CHEMTAX analysis. First, this method requires strong a priori knowledge of the studied phytoplankton communities so that appropriate input ratios and groups are selected. Unfortunately, this is rarely possible, and cryptic or mixotrophic species with endosymbionts (see Vishnu et al., 2022) are always present which adds misclassifications and errors to results. These uncertainties are generally not well resolved, but here, care was taken to select groups and ratios used successfully by other authors (Peña et al., 2019), and our results were in line with expected conditions (Konik et al., 2024). Second, CHEMTAX assumes consistent pigment ratios; however, pigment ratios can be highly variable due to a variety of factors such as light and nutrient conditions (Swan et al., 2016). Here, this influence was likely minimal due to the low variability of winter light and nutrient conditions, and the clustering method we deployed to group and analyze samples with similar ratios. Finally, the broadly utilized satellite groups derived in this study will need to be adapted for temporally resolved data. For example, the Diatoms/Dino/GA grouping was a consequence of these groups showing increased importance in the coastal samples collected under winter conditions; however, during spring and summer, the temporal trends of these groups diverge, with diatom-dominated spring blooms often followed by succession to flagellate dominated summer conditions (Del Bel Belluz et., 2021; Nemcek et al., 2023; Vishnu et al., 2022). Consequently, the use of this grouping on spring and summer data would likely result in the obscuration of important temporal trends in coastal phytoplankton community compositions.

Additionally, uncertainty arises from inherent issues with EOF model training and the use of OLCI Rrs(λ) data. First, insufficient sample numbers in the EOF-based regression model can add errors to the output retrievals (Bracher et al., 2015). In this study, the number of matchup points (59–61) was in line with those used by other authors using similar approaches (e.g., Bracher et al., 2015; Konik et al., 2024; Lange et al., 2020; Vishnu et al., 2022; Xi et al., 2020). Furthermore, we assessed and reported this uncertainty via the cross-validation

method (Table 2) with the results indicating that a sufficient number of points were used to develop a robust regression model. Second, satellite-derived Rrs(λ) retrievals from clear Case-1 oligotrophic waters have been shown to have 5% uncertainty in the blue band with increases toward the red bands (Hu et al., 2013; Tilstone et al., 2021; Vishnu & Costa, 2023). Finally, our study lacks per-pixel uncertainty estimates for the retrieved phytoplankton groups. A recent study by Xi et al. (2021), which employed a similar EOF-based method, quantified per-pixel uncertainties for phytoplankton groups on a global scale, observing lower uncertainty for diatoms, dinoflagellates, green algae, and haptophytes in oligotrophic waters, with higher uncertainty in coastal areas. In our study, we used Polymer v4.10 to derive Rrs(λ) as the spectral input and the uncertainty estimates of this product are not available. However, future studies utilizing the latest version of Polymer Rrs(λ) would be able to derive per-pixel uncertainty for the retrieved phytoplankton groups.

The last limitation of our study was the temporal constraints of our sampling, with data restricted to the winters of 2019 and 2020 as part of the International Year of Salmon Expedition. This expedition was a collaborative effort between Canada, Japan, Korea, the United States, and Russia, and aimed to investigate winter foraging conditions of Pacific salmon across the northeastern Pacific. Our results are novel as phytoplankton abundance and community composition from this region during winter conditions are scarce, making the results of this study unique and notable. While our study is limited temporally and lacks spatial cohesiveness between years, our results are important contributions to understanding winter phytoplankton community dynamics in these waters.

5. Conclusion

Here, we combined in situ CHEMTAX analysis of pigment data with Sentinel-3 OLCI data to derive the spatio-temporal distribution of phytoplankton community composition in the subarctic northeast Pacific during the winter-early spring of 2019 and 2020. This study was part of the International Year of Salmon Expedition, a collaborative effort between Canada, Japan, Korea, the United States, and Russia, and aimed to investigate winter foraging conditions of Pacific salmon across the northeastern Pacific. The Sentinel-3 OLCI EOF-based algorithm showed potential for deriving multiple phytoplankton groups, allowing for considerably greater spatio-temporal resolution than ship-based measurements, including the CHEMTAX-derived data utilized in this study. Specifically, our results showed good retrievals for TChla and the Hapto/Pelago/Cyano groups, with the satellite data largely following the expected trends of homogenous phytoplankton communities dominated by haptophytes over the oceanic northeast Pacific. However, there were departures from this homogeneity, with some groups showing latitudinal and longitudinal variability. Notably, our satellite retrievals indicated an increase in cryptophytes, but also Diatoms/Dino/GA, and TChla toward the northern limits of the study area in 2019. The increases may have resulted from winter marine heatwave conditions and associated low MLDs coupled with the presence of mesoscale eddies and/or the position of the ACC transition zone. In 2020, elevated levels of Diatoms/Dino/GA and TChla were observed near the Haida Gwaii shelf, alongside corresponding decreases in Hapto/Pelago/Cyano and were associated with coastal water masses with lower MLDs and SSS. Both of these findings were consistent with in situ CHEMTAX-derived outputs.

Our results suggest that regional phytoplankton distribution can vary during light-limiting winter conditions when homogenous communities were expected. This variability was effectively documented using Sentinel-3 OLCI imagery, which provided us with comprehensive synoptic data on phytoplankton community composition across extensive spatio-temporal scales, especially during winter when ship-based data for the SNEP is limited. Although we identified some limitations within this data set, the combination with in situ HPLC pigment and physicochemical data provided valuable new insights into regional phytoplankton dynamics during the winter/early spring period in the SNEP. In situ data collected through traditional ship-based surveys remain essential, but observations from ocean color satellites can successfully complement their limited spatio-temporal scale. Algorithms that utilize satellite reflectance to derive phytoplankton community compositions are in their infancy. However, we anticipate significant advancements in the near future with the hyperspectral reflectance data from the recently launched PACE OCI, which is expected to improve the retrieval of these complex aquatic communities.

Deriving phytoplankton community composition using satellite data is extremely important for regions such as the SNEP as they provide habitat for commercially, culturally, and economically important fish species, including Pacific salmon originating from Canada, the United States, Japan, Russia, and Korea. Many recent studies have shown important links between phytoplankton and upper trophic levels in British Columbia waters (i.e., Malick

et al., 2015; Suchy et al., 2022); however, most of these studies are constrained to coastal regions and little is known about these relationships in the open ocean. Here, we show that open ocean waters generally display expected homogeneous phytoplankton community composition during winter conditions; however, there were unexpected exceptions and increased monitoring using high spatio-temporal resolution satellite imagery could further highlight differences from expected conditions. Increases in winter phytoplankton biomass and changes in community composition from factors such as marine heatwaves and eddies could have profound influences on food availability to higher trophic level species such as Pacific salmon.

Data Availability Statement

All physicochemical data used in this study—including sea surface temperature (SST), sea surface salinity (SSS), dissolved oxygen (DO), nutrient concentrations, and HPLC pigment data—are publicly available through the International Year of Salmon (IYS) Data Mobilization Portal under their respective categories:

- SST: https://data.npafc.org/dataset/?eov=subSurfaceTemperature
- SSS: https://data.npafc.org/dataset/?eov=subSurfaceSalinity
- DO: https://data.npafc.org/dataset/?eov=oxygen
- Nutrients: https://data.npafc.org/dataset/?eov=subSurfaceSalinity&ecv=nutrients
- HPLC pigments: https://data.npafc.org/dataset/?q=hplc&sort=score+desc%2C+metadata_modified+desc&eov=oceanColour&tags_en=hplc

The Sentinel-3 OLCI imagery utilized in this study is freely accessible via the Copernicus Data Space Ecosystem: https://dataspace.copernicus.eu/analyse/apis/sentinel-hub. The Polymer atmospheric correction algorithm used in processing is available from HYGEOS: https://hygeos.com/en/polymer/.

In addition, the Line-P HPLC pigment data referenced in this study can be accessed through the DFO Canada Open Data Portal: https://open.canada.ca/data/en/dataset/871b0b32-3135-40c8-868e-c5d87800ca76.

Acknowledgments
The authors would like to thank Richard Beamish, Brian Riddell, and the NPAFC secretariat for organizing the 2019 and 2020 Gulf of Alaska expeditions. We acknowledge the scientific members, technicians, and crew members of the research vessels, *Professor Kaganovskiy* and *Pacific Legacy*, for their help and assistance during the expeditions. We also thank Dr Brian Hunt, Natalie Mahara and Jacob Lerner for collecting the water samples and performing the filtration for HPLC pigments during the 2020 expedition. This research was funded by NSERC NCE MEOPAR—Marine Environmental Observation, Prediction, and Response Network; Canadian Space Agency (FAST 18FAVICB09) to Costa; NSERC Discovery Grant to Costa, and B. Hunt's NSERC Discovery Grant (RGPIN-2017-04499). The authors thank the International Year of Salmon for providing payment-in-kind financial support for the fieldwork. Hongyan Xi's and Astrid Bracher's contributions were funded by the Copernicus Marine Service GLOPHYTS project (21036L05B-COP-INNO SCI-9000), and Angelica Peña's contribution was funded by Fisheries and Oceans Canada. Mercator Ocean implements the Copernicus Marine Service in the framework of a delegation agreement with the European Union. Finally, the authors would like to thank Keith Holmes for his help with graphics.

References

Aguilar-Islas, A. M., Séguret, M. J. M., Rember, R., Buck, K. N., Proctor, P., Mordy, C. W., & Kachel, N. B. (2016). Temporal variability of reactive iron over the Gulf of Alaska shelf. *Deep-Sea Research Part II Topical Studies in Oceanography*, *132*, 90–106. https://doi.org/10.1016/j.dsr2.2015.05.004

Alexander, H., Rouco, M., Haley, S. T., Wilson, S. T., Karl, D. M., & Dyhrman, S. T. (2015). Functional group-specific traits drive phytoplankton dynamics in the oligotrophic ocean. *Proceedings of the National Academy of Sciences of the United States of America*, *12*(44), E5972–E5979. https://doi.org/10.1073/pnas.1518165112

Alvain, S., Moulin, C., Dandonneau, Y., & Bréon, F. M. (2005). Remote sensing of phytoplankton groups in case 1 waters from global SeaWiFS imagery. *Deep-Sea Research Part I Oceanographic Research Papers*, *52*(11), 1989–2004. https://doi.org/10.1016/j.dsr.2005.06.015

Amaya, D. J., Miller, A. J., Xie, S. P., & Kosaka, Y. (2020). Physical drivers of the summer 2019 North Pacific marine heatwave. *Nature Communications*, *11*(1), 1–9. https://doi.org/10.1038/s41467-020-15820-w

Beamish, R. J. (2017). What the past tells us about the future of Pacific salmon research. *Fish and Fisheries*, *18*(6), 1161–1175. https://doi.org/10.1111/faf.12231

Beamish, R. J., & Mahnken, C. (2001). A critical size and period hypothesis to explain natural regulation of salmon abundance and the linkage to climate and climate change. *Progress in Oceanography*, *49*(1–4), 423–437. https://doi.org/10.1016/S0079-6611(01)00034-9

Beardall, J., & Raven, J. A. (2004). The potential effects of global climate change on microalgal photosynthesis, growth and ecology. *Phycologia*, *43*(1), 26–40. https://doi.org/10.2216/i0031-8884-43-1-26.1

Beardall, J., & Stojkovic, S. (2006). Microalgae under global environmental change: Implications for growth and productivity, populations and trophic flow. *Science Asia*, *1*(s1), 1–10. https://doi.org/10.2306/scienceasia1513-1874.2006.32(s1).001

Benoiston, A. S., Ibarbalz, F. M., Bittner, L., Guidi, L., Jahn, O., Dutkiewicz, S., & Bowler, C. (2017). The evolution of diatoms and their biogeochemical functions. *Philosophical Transactions of the Royal Society of London B Biological Sciences*, *372*(20160397), 1–10. https://doi.org/10.1098/rstb.2016.0397

Bishop, J. K. B., Davis, R. E., & Sherman, J. T. (2002). Robotic observations of dust storm enhancement of carbon biomass in the North Pacific. *Science*, *298*, 817–820. https://doi.org/10.1126/science.107496

Blanchet, F. G., Legendre, P., & Borcard, D. (2008). Forward selection of explanatory variables. *Ecology*, *89*(9), 2623–2632. https://doi.org/10.1890/07-0986.1

Booth, B. C., Lewin, J., & Postel, J. R. (1993). Temporal variation in the structure of autotrophic and heterotrophic communities in the subarctic Pacific. *Progress in Oceanography*, *32*(1–4), 57–99. https://doi.org/10.1016/0079-6611(93)90009-3

Boyd, P. W., Wong, C. S., Merrill, J., Whitney, F., Snow, J., Harrison, P. J., & Gower, J. (1998). Atmospheric iron supply and enhanced vertical carbon flux in the NE subarctic Pacific: Is there a connection? *Global Biogeochemical Cycles*, *12*(3), 429–441. https://doi.org/10.1029/98GB00745

Bracher, A., Taylor, M. H., Taylor, B., Dinter, T., Röttgers, R., & Steinmetz, F. (2015). Using empirical orthogonal functions derived from remote-sensing reflectance for the prediction of phytoplankton pigment concentrations. *Ocean Science*, *11*(1), 139–158. https://doi.org/10.5194/os-11-139-2015

Bracher, A., Vountas, M., Dinter, T., Burrows, J. P., Röttgers, R., & Peeken, I. (2009). Quantitative observation of cyanobacteria and diatoms from space using PhytoDOAS on SCIAMACHY data. *Biogeosciences*, *6*(5), 751–764. https://doi.org/10.5194/bg-6-751-2009

Brewin, R. J. W., Sathyendranath, S., Hirata, T., Lavender, S. J., Barciela, R. M., & Hardman-Mountford, N. J. (2010). A three-component model of phytoplankton size class for the Atlantic Ocean. *Ecological Modelling*, *221*(11), 1472–1483. https://doi.org/10.1016/j.ecolmodel.2010.02.014

Brewin, R. J. W., Sathyendranath, S., Jackson, T., Barlow, R., Brotas, V., Airs, R., & Lamont, T. (2015). Influence of light in the mixed-layer on the parameters of a three-component model of phytoplankton size class. *Remote Sensing of Environment*, *168*, 437–450. https://doi.org/10.1016/j.rse.2015.07.004

Brickley, P. J., & Thomas, A. C. (2004). Satellite-measured seasonal and inter-annual chlorophyll variability in the Northeast Pacific and Coastal Gulf of Alaska. *Deep-Sea Research Part II Topical Studies in Oceanography*, *51*(1–3), 229–245. https://doi.org/10.1016/j.dsr2.2003.06.003

Brito, A. C., Sá, C., Mendes, C. R., Brand, T., Dias, A. M., Brotas, V., & Davidson, K. (2015). Structure of late summer phytoplankton community in the Firth of Lorn (Scotland) using microscopy and HPLC-CHEMTAX. *Estuarine, Coastal and Shelf Science*, *167*, 86–101. https://doi.org/10.1016/j.ecss.2015.07.006

Budge, S. M., Wang, S. W., Ormseth, O. A., & Rand, K. M. (2022). Foraging ecology of nearshore fishes in the Gulf of Alaska. *Deep-Sea Research Part II Topical Studies in Oceanography*, *195*, 1–13. https://doi.org/10.1016/j.dsr2.2021.105013

Catlett, D., & Siegel, D. A. (2018). Phytoplankton pigment communities can be modeled using unique relationships with spectral absorption signatures in a dynamic coastal environment. *Journal of Geophysical Research: Oceans*, *123*(1), 246–264. https://doi.org/10.1002/2017JC013195

Chavez, F. P., Ryan, J., Lluch-Cota, S. E., & Ñiquen, C. M. (2003). From anchovies to sardines and back: Multidecadal change in the Pacific Ocean. *Science*, *299*(5604), 217–221. https://doi.org/10.1126/science.1075880

Childers, A. R., Whitledge, T. E., & Stockwell, D. A. (2005). Seasonal and interannual variability in the distribution of nutrients and chlorophyll a across the Gulf of Alaska shelf: 1998–2000. *Deep-Sea Research Part II Topical Studies in Oceanography*, *52*(1–2), 193–216. https://doi.org/10.1016/j.dsr2.2004.09.018

Claustre, H., Hooker, S. B., Van Heukelem, L., Berthon, J.-F., Barlow, R., Ras, J., et al. (2004). An intercomparison of HPLC phytoplankton pigment methods using in situ samples: Application to remote sensing and database activities. *Marine Chemistry*, *85*(1–2), 41–61. https://doi.org/10.1016/j.marchem.2003.09.002

Craig, S. E., Jones, C. T., Li, W. K. W., Lazin, G., Horne, E., Caverhill, C., & Cullen, J. J. (2012). Deriving optical metrics of coastal phytoplankton biomass from ocean colour. *Remote Sensing of Environment*, *119*, 72–83. https://doi.org/10.1016/j.rse.2011.12.007

Crawford, W. R. (2005). Heat and fresh water transport by eddies into the Gulf of Alaska. *Deep-Sea Research Part II*, *52*(7–8), 893–908. https://doi.org/10.1016/j.dsr2.2005.02.003

Cullen, J. T., Chong, M., & Ianson, D. (2009). British Columbian continental shelf as a source of dissolved iron to the subarctic northeast Pacific Ocean. *Global Biogeochemical Cycles*, *23*(GB4012), 1–12. https://doi.org/10.1029/2008GB003326

Cury, P., Shin, Y., Planque, B., Durant, J., Fromentin, J., Kramerschadt, S., et al. (2008). Ecosystem oceanography for global change in fisheries. *Trends in Ecology & Evolution*, *23*(6), 338–346. https://doi.org/10.1016/j.tree.2008.02.005

Dagg, M., Strom, S., & Liu, H. (2009). High feeding rates on large particles by Neocalanus flemingeri and N. plumchrus, and consequences for phytoplankton community structure in the subarctic Pacific Ocean. *Deep-Sea Research Part I*, *56*(5), 716–726. https://doi.org/10.1016/j.dsr.2008.12.012

Damini, B. Y., Rodrigo Costa, R., Dotto, T. S., Rafael Borges Mendes, C., Camilo Torres-Lasso, J., Azaneu, M. V. C., et al. (2023). Antarctica Slope Front bifurcation eddy: A stationary feature influencing CO2 dynamics in the northern Antarctic Peninsula. *Progress in Oceanography*, *212*(102985), 1–15. https://doi.org/10.1016/j.pocean.2023.102985

Del Bel Belluz, J., Jackson, J. M., Kellogg, C. T. E., Peña, M. A., Giesbrecht, I. J. W., & Hobson, L. A. (2024). Phytoplankton community composition links to environmental drivers across a fjord to shelf gradient on the central coast of British Columbia. *Frontiers in Marine Science*, *11*, 1–22. https://doi.org/10.3389/fmars.2024.1458677

Del Bel Belluz, J., Peña, M. A., Jackson, J. M., & Nemcek, N. (2021). Phytoplankton composition and environmental drivers in the northern strait of Georgia (Salish Sea), British Columbia, Canada. *Estuarine and Coasts*, *44*(1), 1419–1439. https://doi.org/10.1007/s12237-020-00858-2

Di Lorenzo, E., Schneider, N., Cobb, K. M., Franks, P. J. S., Chhak, K., Miller, A. J., et al. (2008). North Pacific Gyre Oscillation links ocean climate and ecosystem change. *Geophysical Research Letters*, *35*(8), 1–6. https://doi.org/10.1029/2007GL032838

Donlon, C., Berruti, B., Buongiorno, A., Ferreira, M., Féménias, P., Frerick, J., et al. (2012). The Global Monitoring for Environment and Security (GMES) Sentinel-3 mission. *Remote Sensing of Environment*, *120*, 37–57. https://doi.org/10.1016/j.rse.2011.07.024

Dragoo, D. E., Renner, H. M., & Kaler, R. S. A. (2017). *Breeding status, population trends and diets of seabirds in Alaska, 2016*. U.S. Fish and Wildlife Service Report AMNWR 2017/06. https://doi.org/10.2307/1521664

Dutkiewicz, S., Cermeno, P., Jahn, O., Follows, M. J., Hickman, A. A., Taniguchi, D. A. A., & Ward, B. A. (2020). Dimensions of marine phytoplankton diversity. *Biogeosciences*, *17*(3), 609–634. https://doi.org/10.5194/bg-17-609-2020

Endo, H., Ogata, H., & Suzuki, K. (2018). Contrasting biogeography and diversity patterns between diatoms and haptophytes in the central Pacific Ocean. *Scientific Reports*, *8*(1), 1–13. https://doi.org/10.1038/s41598-018-29039-9

Evans, G. T., & Parslow, J. S. (1985). A model of annual plankton cycles. *Biological Oceanography*, *3*, 327–347. https://doi.org/10.1016/0198-0254(85)92902-4

Falkowski, P. G., & Oliver, M. J. (2007). Mix and match: How climate selects phytoplankton. *Nature Reviews Microbiology*, *5*(10), 813–819. https://doi.org/10.1038/nrmicro1751

Fiechter, J., & Moore, A. M. (2009). Interannual spring bloom variability and Ekman pumping in the coastal Gulf of Alaska. *Journal of Geophysical Research*, *114*(6), 1–19. https://doi.org/10.1029/2008JC005140

Fujiki, T., Matsumoto, K., Honda, M. C., Kawakami, H., & Watanabe, S. (2009). Phytoplankton composition in the subarctic North Pacific during autumn 2005. *Journal of Plankton Research*, *31*(2), 179–191. https://doi.org/10.1093/plankt/fbn108

Giannini, F., Hunt, B. P. V., Jacoby, D., & Costa, M. (2021). Performance of OLCI Sentinel-3A satellite in the Northeast Pacific coastal waters. *Remote Sensing of Environment*, *256*(January), 1–22. https://doi.org/10.1016/j.rse.2021.112317

Goela, P. C., Danchenko, S., Icely, J. D., Lubian, L. M., Cristina, S., & Newton, A. (2014). Using CHEMTAX to evaluate seasonal and interannual dynamics of the phytoplankton community off the south-west coast of Portugal. *Estuarine, Coastal and Shelf Science*, *151*, 112–123. https://doi.org/10.1016/j.ecss.2014.10.001

Grasshoff, K., Kremling, K., & Ehrhardt, M. (1999). In K. Grasshoff, K. Kremling, & M. Ehrhardt (Eds.), *Methods of Seawater Analysis*, *Third*. Wiley VCH.

Gregg, W. W., & Casey, N. W. (2007). Modeling coccolithophores in the global oceans. *Deep Sea Research Part II: Topical Studies in Oceanography*, *54*(5–7), 447–477. https://doi.org/10.1016/j.dsr2.2006.12.007

Hamme, R. C., Webley, P. W., Crawford, W. R., Whitney, F. A., Degrandpre, M. D., Emerson, S. R., et al. (2010). Volcanic ash fuels anomalous plankton bloom in subarctic Northeast Pacific. *Geophysical Research Letters*, *37*(19), 1–5. https://doi.org/10.1029/2010GL044629

Harrison, P. J., Whitney, F. A., Tsuda, A., Saito, H., & Tadokoro, K. (2004). Nutrient and plankton dynamics in the NE and NW Gyres of the subarctic Pacific Ocean. *Journal of Oceanography*, *60*(3), 93–117. https://doi.org/10.1023/B:JOCE.0000038321.57391.2a

Henson, S. A. (2007). Water column stability and spring bloom dynamics in the Gulf of Alaska. *Journal of Marine Research*, *65*(6), 715–736. https://doi.org/10.1016/b978-0-408-70700-8.50018-5

Higgins, H. W., Wright, S. W., & Schlüter, L. (2011). Quantitative interpretation of chemotaxonomic pigment data. In S. Roy, C. A. Llewellyn, E. S. Egeland, & G. Johnsen (Eds.), *Phytoplankton Pigments: Characterization, Chemotaxonomy and Applications in Oceanography* (pp. 257–313). Cambridge University Press. https://doi.org/10.1017/cbo9780511732263.010

Hirata, T., Hardman-Mountford, N. J., Brewin, R. J. W., Aiken, J., Barlow, R., Suzuki, K., et al. (2011). Synoptic relationships between surface Chlorophyll-a and diagnostic pigments specific to phytoplankton functional types. *Biogeosciences*, *8*(2), 311–327. https://doi.org/10.5194/bg-8-311-2011

Hood, R. R., Laws, E. A., Armstrong, R. A., Bates, N. R., Brown, C. W., Carlson, C. A., et al. (2006). Pelagic functional group modeling: Progress, challenges and prospects. *Deep-Sea Research Part II Topical Studies in Oceanography*, *53*(5–7), 459–512. https://doi.org/10.1016/j.dsr2.2006.01.025

Hu, C., Feng, L., & Lee, Z. (2013). Uncertainties of SeaWiFS and MODIS remote sensing reflectance: Implications from clear water measurements. *Remote Sensing of Environment*, *133*, 168–182. https://doi.org/10.1016/j.rse.2013.02.012

Jackson, J. M., Thomson, R. E., Brown, L. N., Willis, P. G., & Borstad, G. A. (2015). Satellite chlorophyll off the British Columbia coast, 1997–2010. *Journal of Geophysical Research: Oceans*, *120*(7), 4709–4728. https://doi.org/10.1002/jgrc.20224

Johnson, S. W., Neff, A. D., Thedinga, J. F., Lindeberg, M. R., & Maselko, J. M. (2012). *Atlas of nearshore fishes of Alaska: A synthesis of marine surveys from 1998 to 2011* (p. 261). U.S. Department of Commerce, NOAA Technical Memorandum NMFS-AFSC-239.

Johnson, W. K., Miller, L. A., Sutherland, N. E., & Wong, C. S. (2005). Iron transport by mesoscale Haida eddies in the Gulf of Alaska. *Deep-Sea Research Part II*, *52*, 933–953. https://doi.org/10.1016/j.dsr2.2004.08.017

Juranek, L. W., White, A. E., Dugenne, M., Freitas, F. H., Dutkiewicz, S., Ribalet, F., et al. (2020). The importance of the phytoplankton "middle class" to ocean net community production. *Global Biogeochemical Cycles*, *34*(12). https://doi.org/10.1029/2020GB006702

Kelley, D., & Richards, C. (2021). gsw: Gibbs sea water functions. Retrieved from https://cran.r-project.org/web/packages/gsw/index.html

Konik, M., Angelica Peña, M., Hirawake, T., Hunt, B. P. V., Suseelan Vishnu, P., Eisner, L. B., et al. (2024). Bioregionalization of the subarctic Pacific based on phytoplankton phenology and composition. *Progress in Oceanography*, *228*, 103315. https://doi.org/10.1016/j.pocean.2024.103315

Kostadinov, T. S., Siegel, D. A., & Maritorena, S. (2009). Retrieval of the particle size distribution from satellite ocean color observations. *Journal of Geophysical Research*, *114*(9), 1–22. https://doi.org/10.1029/2009JC005303

Kostadinov, T. S., Siegel, D. A., & Maritorena, S. (2010). Global variability of phytoplankton functional types from space: Assessment via the particle size distribution. *Biogeosciences*, *7*(10), 3239–3257. https://doi.org/10.5194/bg-7-3239-2010

Kramer, S. J., & Siegel, D. A. (2019). How can phytoplankton pigments be best used to characterize surface ocean phytoplankton groups for ocean color remote sensing algorithms? *Journal of Geophysical Research: Oceans*, *124*(11), 7557–7574. https://doi.org/10.1029/2019JC015604

Kramer, S. J., Siegel, D. A., & Graff, J. R. (2020). Phytoplankton community composition determined from co-variability among phytoplankton pigments from the NAAMES field campaign. *Frontiers in Marine Science*, *7*(215), 1–15. https://doi.org/10.3389/fmars.2020.00215

Landry, M. R., Monger, B. C., & Selph, K. E. (1993). Time-dependency of microzooplankton grazing and phytoplankton growth in the subarctic Pacific. *Progress in Oceanography*, *32*(1–4), 205–222. https://doi.org/10.1016/0079-6611(93)90014-5

Lange, P. K., Werdell, P. J., Erickson, Z. K., Dallamo, G., Brewin, R. J. W., Zubkov, M. V., et al. (2020). Radiometric approach for the detection of picophytoplankton assemblages across oceanic fronts. *Optics Express*, *28*(18), 25682–25705. https://doi.org/10.1364/OE.398127

Legendre, L. (1990). The significance of microalgal blooms for fisheries and for the export of particulate organic carbon in oceans. *Journal of Plankton Research*, *12*(4), 681–699. https://doi.org/10.1093/plankt/12.4.681

Legendre, L., & Legendre, P. (1998). *Numerical ecology* (2nd ed.). Elsevier Science.

Legendre, P., & Gallagher, E. D. (2001). Ecologically meaningful transformations for ordination of species data. *Oecologia*, *129*(2), 271–280. https://doi.org/10.1007/s004420100716

Le Quéré, C., Harrison, S. P., Prentice, I. C., Buitenhuis, E. T., Aumounts, O., Bopp, L., et al. (2005). Ecosystem dynamics based on plankton functional types for global ocean biogeochemistry models. *Global Change Biology*, *11*, 2016–2040. https://doi.org/10.1111/j.1365-2486.2005.01004.x

Lippiatt, S. M., Lohan, M. C., & Bruland, K. W. (2010). The distribution of reactive iron in northern Gulf of Alaska coastal waters. *Marine Chemistry*, *121*(1–4), 187–199. https://doi.org/10.1016/j.marchem.2010.04.007

Lubac, B., & Loisel, H. (2007). Variability and classification of remote sensing reflectance spectra in the eastern English channel and southern North Sea. Remote sensing of coastal aquatic environments. *Technologies, Techniques and Applications*, *110*(2), 45–58. https://doi.org/10.1016/j.rse.2007.02.012

Mackey, M. D., Mackey, D. J., Higgins, H. W., & Wright, S. W. (1996). CHEMTAX—A program for estimating class abundances from chemical markers: Application to HPLC measurements of phytoplankton. *Marine Ecology Progress Series*, *144*(1–3), 265–283. https://doi.org/10.3354/meps144265

MacNeil, L., Costa, M., & LaRoche, J. (2024). Glimpsing the 2020 spring bloom in the Strait of Georgia (Canada) with autonomous ferry-based sensors. *Marine Ecology Progress Series*, *736*, 181–187. https://doi.org/10.3354/meps14574

Maldonado, M. T., Boyd, P. W., Harrison, P. J., & Price, N. M. (1999). Co-limitation of phytoplankton growth by light and Fe during winter in the NE subarctic Pacific Ocean. *Deep Sea Research Part II: Topical Studies in Oceanography*, *46*(11–12), 2475–2485. https://doi.org/10.1016/S0967-0645(99)00072-7

Malick, M. J., Cox, S. P., Mueter, F. J., & Peterman, R. M. (2015). Linking phytoplankton phenology to salmon productivity along a north-south gradient in the Northeast Pacific Ocean. *Canadian Journal of Fisheries and Aquatic Sciences*, *72*(5), 697–708. https://doi.org/10.1139/cjfas-2014-0298

Marañón, E., Cermeño, P., Latasa, M., & Tadonléké, R. D. (2012). Temperature, resources, and phytoplankton size structure in the ocean. *Limnology & Oceanography*, *57*(5), 1266–1278. https://doi.org/10.4319/lo.2012.57.5.1266

Marchese, C., Hunt, B. P. V., Giannini, F., Ehrler, M., & Costa, M. (2022). Bioregionalization of the coastal and open oceans of British Columbia and Southeast Alaska based on Sentinel-3A satellite-derived phytoplankton seasonality. *Frontiers in Marine Science*, *9*(968470), 1–22. https://doi.org/10.3389/fmars.2022.968470

Marchetti, A., Juneau, P., Whitney, F. A., Wong, C. S., & Harrison, P. J. (2006). Phytoplankton processes during a mesoscale iron enrichment in the NE subarctic Pacific: Part II-nutrient utilization. *Deep-Sea Research Part II Topical Studies in Oceanography*, *53*(20–22), 2114–2130. https://doi.org/10.1016/j.dsr2.2006.05.031

Margalef, R. (1995). Life-forms of phytoplankton as survival alternative in an unstable environment. *Acta Oceanologica Sinica*, *1*(4), 493–509.

Martin, l. H., Gordon, R. M., & Fitzwater, S. E. (1991). The case for iron. *Limnology & Oceanography*, *36*(8), 1793–1802. https://doi.org/10.4319/lo.1991.36.8.1793

Matua, N. J., & Hare, S. R. (2002). The Pacific Decadal Oscillation. *Journal of Oceanography*, *58*(1), 35–44. https://doi.org/10.1023/A:1015820616384

McClain, C. R. (2009). A decade of satellite ocean color observations. *Annual Review of Marine Science*, *1*(8), 19–42. https://doi.org/10.1146/annurev.marine.010908.163650

McGowan, D. W., Horne, J. K., & Parker-Stetter, S. L. (2019). Variability in species composition and distribution of forage fish in the Gulf of Alaska. *Deep-Sea Research Part II Topical Studies in Oceanography*, *165*, 221–237. https://doi.org/10.1016/j.dsr2.2016.11.019

Mendes, C. R. B., Costa, R. R., Ferreira, A., Jesus, B., Tavano, V. M., Dotto, T. S., et al. (2023). Cryptophytes: An emerging algal group in the rapidly changing Antarctic Peninsula marine environments. *Global Change Biology*, *29*(7), 1791–1808. https://doi.org/10.1111/gcb.16602

Mendes, C. R. B., Tavano, V. M., Dotto, T. S., Kerr, R., de Souza, M. S., Garcia, C. A. E., & Secchi, E. R. (2018). New insights on the dominance of cryptophytes in Antarctic coastal waters: A case study in Gerlache strait. *Deep-Sea Research Part II Topical Studies in Oceanography*, *149*, 161–170. https://doi.org/10.1016/j.dsr2.2017.02.010

Mendes, C. R. B., Tavano, V. M., Leal, M. C., de Souza, M. S., Brotas, V., & Garcia, C. A. E. (2013). Shifts in the dominance between diatoms and cryptophytes during three late summers in the Bransfield Strait (Antarctic Peninsula). *Polar Biology*, *36*(4), 537–547. https://doi.org/10.1007/s00300-012-1282-4

Miller, C. B. (1993). Pelagic production processes in the Subarctic Pacific. *Progress in Oceanography*, *32*(1), 1–15. https://doi.org/10.1016/0079-6611(93)90007-z

Mograne, M. A., Jamet, C., Loisel, H., Vantrepotte, V., Mériaux, X., & Cauvin, A. (2019). Evaluation of five atmospheric correction algorithms over French optically-complex waters for the Sentinel-3A OLCI Ocean Color Sensor. *Remote Sensing*, *11*(6), 1–25. https://doi.org/10.3390/rs11060668

Mojica, K. D. A., Van De Poll, W. H., Kehoe, M., Huisman, J., Timmermans, K. R., Buma, A. G. J., et al. (2015). Phytoplankton community structure in relation to vertical stratification along a north-south gradient in the Northeast Atlantic Ocean: Phytoplankton and vertical stratification. *Limnology & Oceanography*, *60*(5), 1498–1521. https://doi.org/10.1002/lno.10113

Mueller, J. L., Bidigare, R. R., Trees, C., Balch, W. M., Dore, J., Drapeau, D. T., et al. (2003). Ocean optics protocols for satellite ocean color sensor validation, *Revision 5: Biogeochemical and bio-optical measurements and data analysis protocols*. J. L. Mueller, G. S. Fargion, & C. R. McClain, (Eds.) (Vol. 5). Retrieved from http://oceancolor.gsfc.nasa.gov/cms/techdocs

Nemcek, N., Hennekes, M., Sastri, A., & Perry, R. I. (2023). Seasonal and spatial dynamics of the phytoplankton community in the Salish Sea, 2015–2019. *Progress in Oceanography*, *217*(103108), 1–19. https://doi.org/10.1016/j.pocean.2023.103108

Nemcek, N., & Peña, A. (2014). *Institute of ocean sciences protocols for phytoplankton pigment analysis by HPLC (Technical Report)* (pp. 1–79). Fisheries and Oceans Canada.

Nishioka, J., Obata, H., Hirawake, T., Kondo, Y., Yamashita, Y., Misumi, K., & Yasuda, I. (2021). A review: Iron and nutrient supply in the subarctic Pacific and its impact on phytoplankton production. *Journal of Oceanography*, *77*(4), 561–587. https://doi.org/10.1007/s10872-021-00606-5

Okkonen, S. R., Weingartner, T. J., Danielson, S. L., Musgrave, D. L., & Schmidt, G. M. (2003). Musgrave Satellite and hydrographic observations of eddy-induced shelf-slope exchange in the northwestern Gulf of Alaska. *Journal of Geophysical Research*, *108*(3033), 1–15. https://doi.org/10.1029/2002JC001342

Pakhomov, E. A., Figurkin, A., Hunt, B. P. V., Somov, A., Mahara, N., & International Team 2019–2020. (2022). Oceanographic conditions during the Gulf of Alaska 2019 and 2020 expeditions. *North Pacific Anadromous Fish Commission Technical Report*, *18*, 20–24. https://doi.org/10.23849/npafctr18/20.24

Pan, B. J., Vernet, M., Manck, L., Forsch, K., Ekern, L., Mascioni, M., et al. (2020). Environmental drivers of phytoplankton taxonomic composition in an Antarctic fjord. *Progress in Oceanography*, *183*(102295), 1–20. https://doi.org/10.1016/j.pocean.2020.102295

Peña, A., & Nemcek, N. (2020). Nutrient and phytoplankton along the line p in state of the physical, biological and selected fishery resources of Pacific Canadian marine ecosystems in 2019. In J. L. Boldt, A. Javorski, & P. C. Chandler (Eds.), *Canadian Technical Report of Fisheries and Aquac*. Fisheries & Oceans Canada Institute Ocean Sciences.

Peña, A., & Nemcek, N. (2021). Nutrient and phytoplankton along the line p in state of the physical, biological and selected fishery resources of Pacific Canadian marine ecosystems in 2020. In J. L. Boldt, A. Javorski, & P. C. Chandler (Eds.), *Canadian Technical Report of Fisheries and Aquac*. Fisheries & Oceans Canada Institute Ocean Sciences.

Peña, M. A., Nemcek, N., & Robert, M. (2019). Phytoplankton responses to the 2014–2016 warming anomaly in the northeast subarctic Pacific Ocean. *Limnology & Oceanography*, *64*(2), 515–525. https://doi.org/10.1002/lno.11056

Peña, M. A., & Varela, D. E. (2007). Seasonal and interannual variability in phytoplankton and nutrient dynamics along Line P in the NE subarctic Pacific. *Progress in Oceanography*, *75*(2), 200–222. https://doi.org/10.1016/j.pocean.2007.08.009

Peterson, T. D., Crawford, D. W., & Harrison, P. J. (2011). Evolution of the phytoplankton assemblage in a long-lived mesoscale eddy in the eastern Gulf of Alaska. *Marine Ecology Progress Series*, *424*, 53–73. https://doi.org/10.3354/meps08943

Peterson, T. D., & Harrison, P. J. (2012). Diatom dynamics in a long-lived mesoscale eddy in the northeast subarctic Pacific Ocean. *Deep-Sea Research Part I Oceanographic Research Papers*, *65*, 157–170. https://doi.org/10.1016/j.dsr.2012.03.007

Petrou, K., Kranz, S. A., Trimborn, S., Hassler, C. S., Ameijeiras, S. B., Sackett, O., et al. (2016). Southern Ocean phytoplankton physiology in a changing climate. *Journal of Plant Physiology*, *203*, 135–150. https://doi.org/10.1016/j.jplph.2016.05.004

Pinckney, J. L. (2010). The fourth SeaWiFS HPLC analysis round-robin experiment (SeaHARRE-4) chapter 11 the USC method. NASA Technical Memorandum.

Plant, J. N., Johnson, K. S., Sakamoto, C. M., Jannasch, H. W., Coletti, L. J., Riser, S. C., & Swift, D. D. (2016). Net community production at Ocean Station Papa observed with nitrate and oxygen sensors on profiling float. *Global Biogeochemical Cycles*, *30*(6), 859–879. https://doi.org/10.1002/2015GB005349

Pramlall, S., Jackson, J. M., Konik, M., & Costa, M. (2023). Merged multi-sensor ocean colour chlorophyll product evaluation for the British Columbia coast. *Remote Sensing*, *15*(3), 687. https://doi.org/10.3390/rs15030687

Pramlall, S., Jackson, J. M., Marchese, C., Suchy, K. D., Hunt, B. P. V., & Costa, M. (2024). Mapping phenoregions and phytoplankton seasonality in Northeast Pacific marine coastal ecosystems via a satellite-based approach. *Progress in Oceanography*, *228*(103336), 1–17. https://doi.org/10.1016/j.pocean.2024.103336

Ramette, A. (2007). Multivariate analyses in microbial ecology. *FEMS Microbiology Ecology*, *62*(2), 142–160. https://doi.org/10.1111/j.1574-6941.2007.00375.x

R Core Team. (2021). *R: A language and environment for statistical computing*. R Foundation for Statistical Computing. Retrieved from https://www.R-project.org/

Ribalet, F., Marchetti, A., Hubbard, K. A., Brown, K., Durkin, C. A., Morales, R., et al. (2010). Unveiling a phytoplankton hotspot at a narrow boundary between coastal and offshore waters. *Proceedings of the National Academy of Sciences*, *107*(38), 16571–16576. https://doi.org/10.1073/pnas.1005638107

Ross, T., & Peña, A. (2022). *Trends in the observations at ocean station P and relevance to the two expeditions (technical report no. 18)* (pp. 70–80). North Pacific Anadromous Fish Commission.

Royer, T. C. (1983). Observations of the Alaska coastal current. In H. G. Gade, A. Edwards, & H. Svendsen (Eds.), *Coastal Oceanography* (1st ed., pp. 9–30). Springer. https://doi.org/10.1007/978-1-4615-6648-9

Sambrotto, R. N., & Lorenzen, C. J. (1987). The Gulf of Alaska: Physical environment and biological resources. In D. W. Hood & S. T. Zimmerman (Eds.), *The Gulf of Alaska: Physical environment and biological resources*, *Ocean assessments division* (pp. 249–282). NOAA. U.S. Department of Commerce.

Schwing, F. B., Murphree, T., DeWitt, L., & Green, P. M. (2002). The evolution of oceanic and atmospheric anomalies in the northeast Pacific during the El Niño and La Niña events of 1995–2001. *Progress in Oceanography*, *54*(1–4), 459–491. https://doi.org/10.1016/S0079-6611(02)00064-2

Scott, J. P., & Werdell, P. J. (2019). Comparing level-2 and level-3 satellite ocean color retrieval validation methodologies. *Optics Express*, *27*(21), 30140–30157. https://doi.org/10.1364/oe.27.030140

Siddon, E. C., De Forest, L. G., Blood, D. M., Doyle, M. J., & Matarese, A. C. (2019). Early life history ecology for five commercially and ecologically important fish species in the eastern and Western Gulf of Alaska. *Deep-Sea Research Part II Topical Studies in Oceanography*, *165*, 7–25. https://doi.org/10.1016/j.dsr2.2016.06.022

Soja-Woźniak, M., Craig, S. E., Kratzer, S., Wojtasiewicz, B., Darecki, M., & Jones, C. T. (2017). A novel statistical approach for ocean colour estimation of inherent optical properties and cyanobacteria abundance in optically complex waters. *Remote Sensing*, *9*, 1–22. https://doi.org/10.3390/rs9040343

Stabeno, P. J., Bell, S., Cheng, W., Danielson, S., Kachel, N. B., & Mordy, C. W. (2016). Long-term observations of Alaska coastal Current in the northern Gulf of Alaska. *Deep-Sea Research Part II Topical Studies in Oceanography*, *132*, 24–40. https://doi.org/10.1016/j.dsr2.2015.12.016

Stabeno, P. J., Bond, N. A., Hermann, A. J., Kachel, N. B., Mordy, C. W., & Overland, J. E. (2004). Meteorology and oceanography of the northern Gulf of Alaska. *Continental Shelf Research*, *24*(7–8), 859–897. https://doi.org/10.1016/j.csr.2004.02.007

Stabeno, P. J., Reed, R. K., & Schumacher, J. D. (1995). The Alaska coastal Current: Continuity of transport and forcing. *Journal of Geophysical Research*, *100*(C2), 2477–2485. https://doi.org/10.1029/94jc02842

Steinmetz, F., Deschamps, P.-Y., & Ramon, D. (2011). Atmospheric correction in presence of sun glint: Application to MERIS. *Optics Express*, *19*(10), 9783–9800. https://doi.org/10.1364/oe.19.009783

Steinmetz, F., Ramon, D., & Deschamps, P.-Y. (2016). ATBD v1—Polymer atmospheric correction algorithm ref: D2.3 date: 23/12/2016 issue: 2.1. PML, United Kingdom.

Stock, C. A., Dunne, J. P., & John, J. G. (2014). Global-scale carbon and energy flows through the marine planktonic food web: An analysis with a coupled physical-biological model. *Progress in Oceanography*, *120*(7), 1–28. https://doi.org/10.1016/j.pocean.2013.07.001

Strom, S. L., Fredrickson, K. A., & Bright, K. J. (2016). Spring phytoplankton in the eastern coastal Gulf of Alaska: Photosynthesis and production during high and low bloom years. *Deep-Sea Research Part II Topical Studies in Oceanography*, *132*, 107–121. https://doi.org/10.1016/j.dsr2.2015.05.003

Strom, S. L., Macri, E. L., & Fredrickson, K. A. (2010). Light limitation of summer primary production in the coastal Gulf of Alaska: Physiological and environmental causes. *Marine Ecology Progress Series*, *402*, 45–57. https://doi.org/10.3354/meps08456

Strom, S. L., & Welschmeyer, N. A. (1991). Pigment-specific rates of phytoplankton growth and microzooplankton grazing in the open subarctic Pacific Ocean. *Limnology & Oceanography*, *36*(1), 50–63. https://doi.org/10.4319/lo.1991.36.1.0050

Suchy, K. D., Le Baron, N., Hilborn, A., Perry, R. I., & Costa, M. (2019). Influence of environmental drivers on spatio-temporal dynamics of satellite-derived chlorophyll a in the Strait of Georgia. *Progress in Oceanography*, *176*(July), 1–17. https://doi.org/10.1016/j.pocean.2019.102134

Suchy, K. D., Young, K., Galbraith, M., Perry, R. I., & Costa, M. (2022). Match/mismatch between phytoplankton and crustacean zooplankton phenology in the Strait of Georgia, Canada. *Frontiers in Marine Science*, *9*, 1–21. https://doi.org/10.3389/fmars.2022.832684

Swan, C. M., Vogt, M., Gruber, N., & Laufkoetter, C. (2016). A global seasonal surface ocean climatology of phytoplankton types based on CHEMTAX analysis of HPLC pigments. *Deep Sea Research Part I: Oceanographic Research Papers*, *109*, 137–156. https://doi.org/10.1016/j.dsr.2015.12.002

Taucher, J., Bach, L. T., Prowe, A. E. F., Boxhammer, T., Kvale, K., & Riebesell, U. (2022). Enhanced silica export in a future ocean triggers global diatom decline. *Nature*, *605*(7911), 696–700. https://doi.org/10.1038/s41586-022-04687-0

Taves, R. C., Janssen, D. J., Peña, M. A., Ross, A. R. S., Simpson, K. G., Crawford, W. R., & Cullen, J. T. (2022). Relationship between surface dissolved iron inventories and net community production during a marine heatwave in the subarctic northeast Pacific. *Environmental Science: Processes & Impacts*, *24*(9), 1460–1473. https://doi.org/10.1039/D2EM00021K

Thomson, R. E., & Krassovski, M. V. (2010). Poleward reach of the California Undercurrent extension. *Journal of Geophysical Research*, *115*(C9), 1–9. https://doi.org/10.1029/2010JC006280

Tilstone, G. H., Pardo, S., Dall'Olmo, G., Brewin, R. J. W., Nencioli, F., Dessailly, D., et al. (2021). Performance of ocean colour chlorophyll a algorithms for Sentinel-3 OLCI, MODIS-Aqua and Suomi-VIIRS in open-ocean waters of the Atlantic. *Remote Sensing of Environment*, *260*(112444), 1–19. https://doi.org/10.1016/j.rse.2021.112444

Tréguer, P., Bowler, C., Moriceau, B., Dutkiewicz, S., Gehlen, M., Aumont, O., et al. (2018). Influence of diatom diversity on the ocean biological carbon pump. *Nature Geoscience*, *11*(1), 27–37. https://doi.org/10.1038/s41561-017-0028-x

Trudel, M., Moss, J. H., Tucker, S., Candy, J. R., & Beacham, T. D. (2011). Stock-specific distribution of juvenile sockeye salmon in the eastern Gulf of Alaska. *North Pacific Anadromous Fish Commission Document*, *1353*, 11.

Ueno, H., Bracco, A., Barth, J. A., Budyansky, M. V., Hasegawa, D., Itoh, S., et al. (2023). Review of oceanic mesoscale processes in the North Pacific: Physical and biogeochemical impacts. *Progress in Oceanography*, *212*(102955), 1–37. https://doi.org/10.1016/j.pocean.2022.102955

Uitz, J., Claustre, H., Morel, A., & Hooker, S. B. (2006). Vertical distribution of phytoplankton communities in open ocean: An assessment based on surface chlorophyll. *Journal of Geophysical Research*, *111*(8). https://doi.org/10.1029/2005JC003207

Vaillancourt, R. D., Lance, V. P., & Marra, J. F. (2018). Phytoplankton chemotaxonomy within contiguous optical layers across the Western North Atlantic Ocean and its relationship to environmental parameters. *Deep-Sea Research Part I Oceanographic Research Papers*, *139*, 14–26. https://doi.org/10.1016/j.dsr.2018.05.007

Vanni, M. J., & Findlay, D. L. (1990). Trophic cascades and phytoplankton community structure. *Ecology*, *71*(3), 921–937. https://doi.org/10.2307/1937363

Vinogradov, M. E., Shushkina, E. A., Vedernikov, V. I., Nezlin, N. P., & Gagarin, V. I. (1997). Primary production and plankton stocks in the Pacific Ocean and their seasonal variation according to remote sensing and field observations. *Deep-Sea Research Part II Topical Studies in Oceanography*, *44*(9–10), 1979–2001. https://doi.org/10.1016/S0967-0645(97)00086-6

Vishnu, P. S., & Costa, M. (2023). Evaluating the performance of Sentinel-3A OLCI products in the subarctic northeast Pacific. *Remote Sensing*, *15*(13), 3244. https://doi.org/10.3390/rs15133244

Vishnu, P. S., Xi, H., Belluz, J. D. B., Hussain, M. S., Bracher, A., & Costa, M. (2022). Seasonal dynamics of major phytoplankton functional types in the coastal waters of the west coast of Canada derived from OLCI Sentinel 3A. *Frontiers in Marine Science*, *9*, 1018510. https://doi.org/10.3389/fmars.2022.1018510

Waite, J. N., & Mueter, F. J. (2013). Spatial and temporal variability of chlorophyll-a concentrations in the coastal Gulf of Alaska, 1998–2011, using cloud-free reconstructions of SeaWiFS and MODIS-Aqua data. *Progress in Oceanography*, *116*, 179–192. https://doi.org/10.1016/j.pocean.2013.07.006

Weingartner, T. (2006). In R. B. Speis (Ed.), *"Long-term ecological change in the northern gulf of Alaska": The Physical Environment of the Gulf of Alaska*. Elsevier.

Weingartner, T., Coyle, K., Finney, B., Hopcroft, R., Whitledge, T., Brodeur, R., et al. (2002). The Northeast Pacific GLOBEC program: Coastal Gulf of Alaska. *Oceanography*, *15*(2), 48–63. https://doi.org/10.5670/oceanog.2002.21

Weingartner, T., Eisner, L., Eckert, G. L., & Danielson, S. (2009). Southeast Alaska: Oceanographic habitats and linkages. *Journal of Biogeography*, *36*(3), 387–400. https://doi.org/10.1111/j.1365-2699.2008.01994.x

Welschmeyer, N. A., Strom, S., Goericke, R., DiTullio, G., Belvin, M., & Petersen, W. (1993). Primary production in the subarctic Pacific ocean: Project SUPER. *Progress in Oceanography*, *32*(1–4), 101–135. https://doi.org/10.1016/0079-6611(93)90010-B

Werdell, P. J., & Bailey, S. W. (2005). An improved in-situ bio-optical data set for ocean color algorithm development and satellite data product validation. *Remote Sensing of Environment*, *98*(1), 122–140. https://doi.org/10.1016/j.rse.2005.07.001

Werdell, P. J., Roesler, C. S., & Goes, J. I. (2014). Discrimination of phytoplankton functional groups using an ocean reflectance inversion model. *Applied Optics*, *53*(22), 4833–4849. https://doi.org/10.1364/AO.53.004833

Westberry, T. K., Schultz, P., Behrenfeld, M. J., Dunne, J. P., Hiscock, M. R., Maritorena, S., et al. (2016). Annual cycles of phytoplankton biomass in the subarctic Atlantic and Pacific Ocean. *Global Biogeochemical Cycles*, *30*(1), 175–190. https://doi.org/10.1002/2015GB005276

Whitney, F. A., Crawford, W. R., & Harrison, P. J. (2005). Physical processes that enhance nutrient transport and primary productivity in the coastal and open ocean of the subarctic NE Pacific. *Deep-Sea Research Part II Topical Studies in Oceanography*, *52*(5–6), 681–706. https://doi.org/10.1016/j.dsr2.2004.12.023

Wickham, H. (2016). In R. Gentleman, G. Parmigiani, & K. Hornik (Eds.), *Ggplot2: Elegant graphics for data analysis*. Springer. https://doi.org/10.1007/978-0-387-78171-6

Womble, J. N., & Sigler, M. F. (2006). Seasonal availability of abundant, energy-rich prey influences the abundance and diet of a marine predator, the Steller sea lion Eumetopias jubatus. *Marine Ecology Progress Series*, *325*, 281–293. https://doi.org/10.3354/meps325281

Womble, J. N., Sigler, M. F., & Willson, M. F. (2009). Linking seasonal distribution patterns with prey availability in a central-place forager, the Steller sea lion. *Journal of Biogeography*, *36*(3), 439–451. https://doi.org/10.1111/j.1365-2699.2007.01873.x

Wood, E. D., Armstrong, F. A. J., & Richards, F. A. (1967). Determination of nitrate in sea water by cadmium-copper reduction to nitrite. *Journal of the Marine Biological Association of the United Kingdom*, *47*(1), 23–31. https://doi.org/10.1017/S002531540003352X

Wright, S. W., Ishikawa, A., Marchant, H. J., Davidson, A. T., Enden, R. L. v. d., & Nash, G. V. (2009). Composition and significance of picophytoplankton in Antarctic waters. *Polar Biology*, *32*(5), 797–808. https://doi.org/10.1007/s00300-009-0582-9

Xi, H., Losa, S. N., Mangin, A., Garnesson, P., Bretagnon, M., Demaria, J., et al. (2021). Global chlorophyll a concentrations of phytoplankton functional types with detailed uncertainty assessment using multisensor ocean color and sea surface temperature satellite products. *Journal of Geophysical Research: Oceans*, *126*(5), 1–27. https://doi.org/10.1029/2020jc017127

Xi, H., Losa, S. N., Mangin, A., Soppa, M. A., Garnesson, P., Demaria, J., et al. (2020). Global retrieval of phytoplankton functional types based on empirical orthogonal functions using CMEMS GlobColour merged products and further extension to OLCI data. *Remote Sensing of Environment*, *240*, 1–21. https://doi.org/10.1016/j.rse.2020.111704

Yang, B., Emerson, S. R., & Angelica Peñã, M. (2018). The effect of the 2013–2016 high temperature anomaly in the subarctic Northeast Pacific (the "blob") on net community production. *Biogeosciences*, *15*(21), 6747–6759. https://doi.org/10.5194/bg-15-6747-2018

Zhang, H. R., Wang, Y., Xiu, P., Qi, Y., & Chai, F. (2021). Roles of iron limitation in phytoplankton dynamics in the Western and eastern subarctic Pacific. *Frontiers in Marine Science*, *8*, 1–18. https://doi.org/10.3389/fmars.2021.735826